Inhibition of ACSL4 ameliorates tubular ferroptotic cell death and protects against fibrotic kidney disease

Yue Dai
Tongji Hospital   https://orcid.org/0000-0002-4388-0496

Yuting Chen
Tongji Hospital   https://orcid.org/0000-0001-6209-1890

Dexiameng Mo
Tongji Hospital

Rui Jin
Tongji Hospital

Yi Huang
Tongji Hospital

Le Zhang
Tongji Hospital

Cuntai Zhang
Tongji Hospital

Hongyu Gao
Tongji hospital   https://orcid.org/0000-0002-7462-8883

Qi Yan (✉ yanqi@tjh.tjmu.edu.cn)
Tongji Hospital   https://orcid.org/0000-0001-9542-5607

Article

Additional Declarations: (Not answered)

Inhibition of ACSL4 ameliorates tubular ferroptotic cell death and protects against fibrotic kidney disease

Yue Dai[#], Yuting Chen[#], Dexiameng Mo, Rui Jin, Yi Huang, Le Zhang, Cuntai Zhang, Hongyu Gao[*], Qi Yan [*]

Department of Geriatrics, Tongji Hospital, Tongji Medical College, Huazhong University of Science and Technology, Wuhan, China

*Corresponding authors:

Hongyu Gao, Ph. D, M.D. Department of Geriatrics, Tongji Hospital, Tongji Medical College, Huazhong University of Science and Technology, Jiefang Road 1095#, Qiaokou District, Wuhan, 430030, China. Tel.: 086-13886188018; Fax: 086-027-83663035; E-mail: hygao@tjh.tjmu.edu.cn.

Qi Yan, Ph. D, M.D. Department of Geriatrics, Tongji Hospital, Tongji Medical College, Huazhong University of Science and Technology, Jiefang Road 1095#, Qiaokou District, Wuhan, 430030, China. Tel.: 086-15377013277; Fax: 086-027-83663035; E-mail: yanqi@tjh.tjmu.edu.cn.

[#]These authors contributed equally: Yue Dai, Yuting Chen.

Running title: Role of ACSL4 in fibrotic kidney

Key words: ACSL4; ferroptosis; tubular epithelial cells; kidney fibrosis; lipid programming

Abbreviation: 4-HEN, 4-hydroxynonenal; α-SMA, α-smooth muscle actin; AA, arachidonic acid; ACSL4, acyl-CoA synthetase long-chain family member 4; AdA, adrenic acid; AKI, acute kidney disease; CKD, chronic kidney disease; DFO, deferoxamine; EMT, epithelial-to-

1 mesenchymal transition; FA, fatty acid; FGF2, fibroblast growth factor 2; FN, fibronectin;

2 GPX4, Glutathione peroxidase 4; HE, hematoxylin-eosin; IHC, Immunohistochemistry;

3 LOOHs, lipid hydroperoxides; LPCAT3, lyso-phosphatidylcholine acyltransferase 3; MTS,

4 Masson's trichrome staining; PAS, periodic acid-Schiff; PDGFB, platelet-derived growth

5 factor subunit B; PE, phosphatidylethanolamine; PUFAs, polyunsaturated free fatty acids;

6 PUFA-OOH: hydroperoxides of polyunsaturated fatty acids; ROS, reactive oxygen species;

7 ROSI, rosiglitazone; RT-PCR, real-time polymerase chain reaction; TECs, tubular epithelial

8 cells; PPARγ, peroxisome proliferator-activated receptor γ; UUO, unilateral ureteral

9 obstruction.

1   **Abstract**

2   Ferroptosis is a recently recognized form of regulated cell death, characterized by iron-

3   dependent accumulation of lipid peroxidation. Ample evidence has depicted that ferroptosis

4   plays an essential role in the cause or consequence of human diseases, including cancer,

5   neurodegenerative disease and acute kidney injury. However, the exact role and underlying

6   mechanism of ferroptosis in fibrotic kidney remain unknown. Acyl-CoA synthetase long-

7   chain family member 4 (ACSL4) has been demonstrated as an essential component in

8   ferroptosis execution by shaping lipid composition. In this study, we aim to discuss the

9   potential role and underlying mechanism of ACSL4-mediated ferroptosis of tubular epithelial

10   cells (TECs) during renal fibrosis. The unbiased gene expression studies showed that ACSL4

11   expression was tightly associated with decreased renal function and the progression of renal

12   fibrosis. To explore the role of ACSL4 in fibrotic kidney, ACSL4 specific inhibitor

13   rosiglitazone (ROSI) was used to disturb the high expression of ACSL4 in TECs induced by

14   TGF-β, unilateral ureteral obstruction (UUO) and fatty acid (FA)-modeled mice, and

15   furthermore we used ACSL4 siRNA to knockdown ACSL4 in TGF-β-induced HK2. The

16   results demonstrated that inhibition and knockdown of ACSL4 effectively attenuated the

17   occurrence of ferroptosis of TECs and alleviated the interstitial fibrotic response. In addition,

18   the expression of various profibrotic cytokines all decreased after ROSI-treated in vivo and in

19   vitro. Further investigation showed that inhibition of ACSL4 significantly attenuates the

20   progression of renal fibrosis by reducing the proferroptotic precursors arachidonic acid- and

21   adrenic acid- containing phosphatidylethanolamine (AA-PE and AdA-PE). In conclusion,

22   these results suggest ACSL4 is essential for tubular ferroptotic death during kidney fibrosis

1   development and ACSL4 inhibition is a viable therapeutic approach to preventing fibrotic

2   kidney diseases.

3   **Key words:** ACSL4; ferroptosis; tubular epithelial cells; kidney fibrosis; lipid

4   reprogramming

5

1   **INTRODUCTION**

2   The incidence and prevalence of chronic kidney disease (CKD) continue to grow and are

3   gradually emerging as one of the leading causes of mortality worldwide[1]. Kidney fibrosis is

4   regarded as the final common pathological manifestation of chronic kidney diseases, and the

5   process characterized by the deposition of extra cellular matrix, the proliferation of interstitial

6   myofibroblasts, interstitial inflammatory response and loss of interstitial capillary integrity[2, 3].

7   It is widely accepted that among the diverse cell types involved in renal fibrosis, tubular

8   epithelial cells (TECs) act as primarily responder to pathological changes in interstitium

9   following early injury and to produce tubulointerstitial fibrosis[4, 5]. Thus, a better

10   understanding of the mechanism of TECs in kidney fibrosis is essential for revealing

11   therapeutic options to prevent the progression of CKD. TECs death is a hallmark feature of

12   renal parenchymal damage, and there is increasing evidence showing that TECs death is the

13   main mechanism of tubular damage, which is also the direct cause of kidney tubulointerstitial

14   fibrosis after injury[6, 7, 8]. Cell cycle arrest, epithelial-to-mesenchymal transition (EMT),

15   metabolic changes, and the loss of TECs can promote the damage in TECs[9]. It has been

16   demonstrated that the depletion of TECs can be activated by regulated cell death, such as

17   apoptosis, necrosis and pyroptosis[10, 11, 12, 13]. With delving into the ways of cell death,

18   ferroptosis was identified as a form of non-apoptotic cell death, which is involved in a lot of

19   pathological processes that include kidney injury[14]. Several studies indicate that ferroptosis is

20   involved in ischemia-reperfusion[15] and folic acid[16] induced kidney injury. There are only a

21   few studies that have confirmed the core role of ferroptosis in CKD. Zhou et al. found that

22   administrating ferroptosis inhibitor ferrostatin-1 ameliorates the extent of UUO-induced renal

5

1 fibrosis in vivo[17]. Iron chelator, deferoxamine (DFO), also rescues the renal fibrosis caused by

2 UUO by inhibiting ferroptosis[18]. Another study found that liproxstatin-1, a ferroptosis

3 inhibitor, plays a protective role in the UUO-induced interstitial fibrosis which may respond

4 by inhibiting the paracrine pathway of profibrotic molecules of TECs[19]. Thus, it is essential to

5 explore the underlying molecular mechanisms of ferroptosis in TECs under renal fibrosis

6 conditions.

7 Ferroptosis is driven by the iron-dependent accumulation of peroxidized lipids[14]. The

8 peroxidation of lipids is an important step in promoting ferroptosis. Increased synthesis of

9 polyunsaturated fatty acids (PUFA) induces lipid peroxidation during ferroptosis. Several

10 products of lipid peroxidation including the initial lipid hydroperoxides (LOOHs) and

11 subsequent reactive aldehydes (e.g., 4-hydroxynonenal (4-HNE)), are increased under

12 ferroptotic stimuli conditions[20, 21]. Previous studies have shown that kidney fibrosis is

13 accompanied by the accumulation of renal lipid peroxides. Liang et al. found that 4-HNE was

14 markedly increased in fibrotic kidney tissues after UUO challenge, suggesting that renal lipid

15 peroxidation may be involved in the activation of ferroptosis during kidney fibrosis[22].

16 Recently, some genes encoding proteins involve in lipid peroxidation for the induction of

17 ferroptosis have been identified. Of such, acyl-CoA synthetase long-chain family member 4

18 (ACSL4) and lyso-phosphatidylcholine acyltransferase 3 (LPCAT3) are confirmed to

19 participate in the biosynthesis and remodeling of PUFA- phosphatidylethanolamines (PEs) in

20 cellular membranes[23, 24]. Loss of these gene products exhausts the substrates for lipid

21 peroxidation and raises resistance to ferroptosis. Of note, arachidonic acid (AA; C20:4) and

22 adrenic acid (AdA; C22:4) are the prime substrates for lipid peroxidation in ferroptosis.

ACSL4 first catalyzes the biochemical reaction of free AA/AdA to CoA into their acyl-CoA esters, while LPCAT3 then facilitates AA re-acylation into lysophospholipids. Doll et al. shows that the expression of ACSL4 is closely related to the sensitivity of breast cancer cells to ferroptotic death[24]. Cancer cells with low expression level of ACSL4 are significantly resistant to ferroptotic death, and have stronger invasiveness and proliferation ability. In intestinal ischemia-reperfusion, ferroptosis of intestinal cells participated in intestinal I/R injury; inhibition of ACSL4 at the gene or pharmacological level effectively improved intestinal tissue damage induced by reperfusion by inhibiting intestinal cell ferroptosis[25]. Recent studies also found that ferroptosis-related genes, including ACSL4, was significantly increased during lung ischemia/reperfusion. Administration of ACSL4 inhibitor before ischemia can reduce the iron death degree of lung tissue and weaken the lung tissue damage caused by ischemia[26]. These studies suggest that targeted intervention of ACSL4 might be a key strategy to regulate the susceptibility of cells to ferroptotic death. However, the specific role of ACSL4 that drives ferroptosis and the downstream of the lipid signals responsible for ferroptosis activation are poorly defined in the context of fibrotic kidney diseases.

In this study, pharmacological inhibition and knockdown of ACSL4 are used to investigate its role in mediating TECs ferroptosis in kidney fibrosis. ACSL4 inhibition alleviate the kidney fibrosis by suppressing ferroptotic TECs. Then, we apply lipidomic to investigate key conditions in the process of lipid biosynthesis. The results suggest that targeting ACSL4 to inhibit AA and AdA esterification to PE is an anti-ferroptosis modality which alleviates fibrotic kidney. This may provide new targets and a theoretical basis for the treatment of CKD by targeting ACSL4 and lipid reprograming

1 **MATERIALS AND METHODS**

2 **Animals**

3 All handlings and experimental procedures of mice were performed in accordance with the

4 guidelines of the National Health and Medical Research Council of China, and the protocol

5 was approved by the animal ethics review board of Tongji Medical College in Huazhong

6 University of Science and Technology (Permit Number: S 2670).

7 Male C57BL/6J mice were fed in a specific pathogen-free (SPF) environment in the

8 laboratory animal center of Tongji Medical College. Animals were given free access to

9 normal diet and acclimatized in a ventilated temperature-controlled room (24 °C), with a

10 regular 12 h light/dark cycle. Male 8–12-week C57BL/6 mice were used in the follow

11 experiments. For unilateral ureteral obstruction (UUO) model, mice underwent left UUO

12 surgery, the left mid-ureter of mice was exposed via a lateral incision and obstructed it twice

13 with 4–0 silk sutures.

14 For folic acid administration model, mice were intraperitoneally injected with a single dose of

15 folic acid (250 mg/kg body weight dissolved in 300 mM NaHCO3). The mice were

16 intraperitoneally treated with ROSI (0.5 mg/kg/day) at 1 h prior to handlings of UUO and FA,

17 and continuously injected daily for UUO and FA duration. After 14 days for UUO model and

18 28 days for FA model, kidney tissues were collected for the further experiments.

19 **Cell lines and culture conditions.**

20 HK-2 (human kidney tubular cell) was obtained from China Centre for Type Culture

21 Collection (CCTCC, China), and maintained in DMEM-F12 (Biological Industries, USA)

22 medium containing 10% fetal bovine serum (FBS) and 1% penicillin-streptomycin. Cells

were incubated in a humidified atmosphere of 95% air and 5% CO2 at 37 °C. At the case of

cells treatment, recombinant human TGF-β (Peprotech, Rocky Hill, NJ) was added at cells for

48h, with the concentration of 20 ng/ml. 100 μM rosiglitazone (Sigma-Aldrich, USA) treated

cells for 48h.

ACSL4 siRNA and control siRNA was purchased from Qiagen (Germany). Transfection was

performed using HiPerFect transfection (Qiagen, Germany) according to the manufacturer's

protocol. The efficiency of transfection was assessed by the protein expression. The sequence

used for knockdown of ACSL4 in this study was: 5′-TTGGAGCGATTTGAAATTCCA -3′.

HK-2 cells treated with or without TGF-β, as well as the cells transfected with ACSL4 siRNA

for 48 h.

Cell viability and cytotoxicity assay

HK-2 cells were cultured with the optimal cell concentration of 1×10^4 cells/well in a 96-

well plate. During TGF-β induced fibrosis, HK-2 cells were treated with rosiglitazone in

different groups for 48 h. For the ACSL4 siRNA treatment experiments, HK-2 cells were

treated with control siRNA, ACSL4 siRNA or TGF-β for 48 h after plating. Cell viability was

measured by MTT (KeyGEN, KGA311, China). MTT were diluted by buffer and added at 96-

well plate with 50 μL/well to incubate 4 h at incubators. Absorbance was detected at 490 nm

after treatment with 150 μL of DMOS reagent for 1 h. Cell cytotoxicity was detected by LDH

(Roche, 04744926001, USA). To determine the LDH activity, we conducted cells according

to the manufacturer's instructions. The absorbance was read at 490 nm and caculated to get

the percentage cytotocicity by the following equation: cytotoxicity(%)=(value of samples -

low control) / (high control – low control) × 100 %.

Cell immunofluorescence assay

HK-2 cells were cultured in 6-well plate format for cell immunofluorescence analysis. After

treatment of rosiglitazone (100 μM) and TGF-β (20 ng/ml) for 48 h, the medium was removed

and cells were cleaned three times with PBS. Cells in coverslips of 6-well plate were fixed in

4% paraformaldehyde for 15 minutes, and then blocked with 10% goat serum (Boster,

AR0009, China) for 1 h before incubation with primary antibodies against 4-HNE (1:100

dilution), Fibronectin (1:250 dilution) and α-SMA (1:250 dilution) at 4°C for 24 h. After

incubation, coverslips were rinsed three times with PBS for 5 minutes and incubated with the

secondary antibodies Dylight 488 goat anti-rabbit IgG (Abbkine, California, USA) and

Dylight 594 goat anti-mouse IgG (Abbkine, California, USA) for 60 minutes at room

temperature. After antifade mounting medium with DAPI (Beyotime, P0131, China), samples

were observed under confocal microscopy (Nikon C2, Japan) and fluorescence intensity was

analyzed using ImageJ software.

BODIPY 581/591 C11 analysis

HK-2 cells were treated with rosiglitazone (100 μM) and TGF-β (20 ng/ml) for 48 h at 6-well

dishes containing 25mm coverslip per well. After treatment, the medium were removed and

cells were washed three times with sterile PBS. Complete medium was used to prepare

BODIPY 581/591 C11 (Thermo Fisher Scientific, D3681, USA) working solution with the

concentration of 5 μM. 6-well dishes were added 1ml per well and incubated at 37°C for 30

minutes in the dark. At the end of the treatment, we removed the medium and cleaned cells

three times with PBS. Glass coverslips with cells were fixed in 4% paraformaldehyde for 15

minutes. Subsequently, coverslips were transferred to glass microscope slide with the antifade

mounting medium with DAPI (Beyotime, P0131, China). The images were captured using

confocal microscopy (Nikon C2, Japan). To quantify the intensity of oxidization, the

background was corrected by subtracting the red or green fluorescence in cell-free areas and

then calculated the ratio of the green fluorescence to red and green fluorescence.

Histological analysis

Excised kidney tissues were fixed in 4% paraformaldehyde, embedded in paraffin and

sectioned for the following experiments. Sections were stained with hematoxylin-eosin (HE),

periodic acid-Schiff (PAS), and Masson's trichrome staining (MTS) according to the standard

protocols. We evaluated the degree of tubular atrophy in line with the renal tubular damage

score, which were based on cast formation, tubular dilation, brush border loss and interstitial

fibrosis, with scores corresponding to the following percentages of renal tubular damage: 0,

0%; 1, ≤10%, 2, 11 to 25%; 3, 26 to 45%; 4, 46 to 75%; and 5, ≥76%. In each sections,

damaged areas were determined in the successive field of entire cortical and juxtamedullary

areas. The total damaged areas under examination using Image J software (National Institutes

of Health, Bethesda, MD) assisted image analysis. MTS was analyzed semi-quantitatively by

quantifying the blue-stained areas of 6 random different views.

Immunohistochemistry (IHC) and immunofluorescence (IF) assay

We performed immunohistochemistry and immunofluorescence in paraffin sections using the

steam-based antigen retrieval technique. Deparaffined sections were used for IHC of GPX4

(Abcam, ab125066, 1:100 dilution, Britain) and IF of 4-HNE (Abcam, ab46545, 1:100

dilution, Britain), α-SMA (Abcam, ab124964,1:250 dilution, Britain) and Fibronectin

(Abcam, ab45688, 1:250 dilution, Britain). Images of IF were acquired on confocal

1   microscopy (Nikon C2, Japan). The samples of IHC were examined using the microscope

2   (Mshot, China). The intensities of the expression of the target gene were detected by Image J

3   software (National Institutes of Health, Bethesda, MD).

4   **Real-time PCR analysis**

5   RNA was extracted from harvested HK-2 cells and kidney tissues using FastPure Cell/Tissue

6   Total RNA Isolation Kit (Vazyme, RC11201, Chinan) and reversely transcribed into cDNA by

7   ReverTra Ace qPCR RT kit (Toyobo, FSQ-101, Japan). The system of real-time polymerase

8   chain reaction (RT-PCR) was mixed by SYBR Green Master and gene-specific primers, and

9   RT-PCR was run in the ABI Step One Plus system (Applied Biosystems, USA). The mRNA

10   expression levels of target genes were normalized and analyzed using the $\Delta\Delta$Ct method. The

11   primers used in this study are listed in **Supplementary Table 1**.

12   **Western Blot and Antibody**

13   Cells and kidney tissues were lysed by sonication in RIPA buffer containing 1% PMSF and

14   1% protease inhibitor. The protein extracts were prepared after measuring the protein

15   concentration by BCA (Boster, AR0146, China) method. Protein samples were measured by

16   western blotting of electrophoresis in 10% SDS-PAGE gel and transferred with PVDF

17   membrane (Millipore, USA). Skim milk was used to block nonspecific signals at room

18   temperature for 1 h. The membranes were incubated by primary antibodies against GPX4

19   (Abcam, ab125066, 1:3000 dilution, Britain), ACSL4 (Santa Cruz, SC393906, 1:1000

20   dilution, USA), LPCAT3(Abcam, ab232958, 1:500 dilution, Britain), Fibronectin (Abcam,

21   ab45688, 1:5000 dilution, Britain), α-SMA (Abcam, ab124964,1:2000 dilution, Britain),

22   Collagen-I (Proteintech, 14695-1-AP,1:1000 dilution, USA), TGF-β1 (Abcam, ab215715,

1:1000 dilution, Britain), p-Smad2 (CST, 3104 S,1:1000 dilution, USA), p-Smad3(CST,

9520T S,1:1000 dilution, USA) and GAPDH (Promoter, 1:25000, China). After washing,

membranes were incubated with Horseradish peroxidase-conjugated anti-mouse and anti-

rabbit (Promoter, 1:5000 dilution, China) at room temperature for 1 h. Immunoblots were

imaged on the UVP imager (UVP, USA). Gray values of specific bands were quantified by

ImageJ software.

Separation and detection of Lipidomic

A LC-MS system consisting of Waters 2D UPLC（Waters, USA）and Q Exactive high

resolution mass spectrometer (Thermo Fisher Scientific, USA) was used for lipids separation

and detection. 800 μL of extract (dichloromethane/methanol=3/1, v/v) and 10 μL of SPLASH

internal standards solution were added in the 1.5mL Eppendorf tube contained the sample to

grind. Supernatant of the sample was taken for lyophilization and econstituted with 200 μL of

reconstitution fluid (Isopropanol/Acetonitrile/Water = 2/1/1, v/v/v). After ultrasonic treatment

and shaking, the supernatant was placed in a 1.5mL vial. To evaluate the repeatability and

stability of LC-MS/MS analysis, 20 μL of supernatant of each sample was mixed into a QC

sample. Lipidomic were analyzed by phase LC-MS/MS. Data of positive-ion and negative-ion

mode was acquired respectively to improve the lipid coverage.

Analysis of Lipidomics by LC-MS/MS

A CSH C18 column (1.7 μm 2.1*100 mm, Waters, USA) was used in this study. Under

positive ion mode, the mobile phase consisted of solvent A (60% acetonitrile aqueous solution

+ 0.1% formic acid + 10 mM ammonium formate) and solvent B (10% acetonitrile aqueous

solution + 90% Isopropanol + 0.1% formic acid + 10 mM ammonium formate). Under

1 negative ion mode, the mobile phase contained solvent A (60% acetonitrile aqueous solution

2 + 10 mM ammonium formate) and solvent B (10% acetonitrile aqueous solution + 90%

3 Isopropanol + 10 mM ammonium formate). The column was eluted in the gradient elution

4 conditions. The flow rate was 0.35 mL/min. The column oven was maintained at 55 °C. The

5 injection volume was 5 μL. A Q Exactive mass spectrometer (Thermo Fisher Scientific, USA)

6 was used to obtain MS1 and MS2 data. The MS scan method was in the range of m/z 200–

7 2000, The MS1 resolution was 70,000 and the maximum injection time was 100 ms.

8 According to the precursor ion intensity, Top 3 ions were selected for MS2 analysis, MS2

9 resolution was 17,500, maximum injection time was 50 ms, and collision energy were set as:

10 15, 30 and 45 eV. The parameters of ESI were sheath gas of 40 L/min, aux gas of 10 L/min,

11 spray voltage of 3.80 in positive ion mode and of 3.20 in negative ion mode, capillary

12 temperature of 320 °C and aux gas heater temperature of 350 °C.

13 **pretreatment of Lipidomics data**

14 Lipidomics data processing by LipidSearch 4.1 that first conducted identification and peak

15 extraction for each sample, and then peak alignment for all samples. The BGI's own

16 metabolomics software package metaX[27] was used for statistical analysis. PCA model was

17 used to observe the inter-group differences of the samples. The variable importance in

18 projection values of the first two principal components of the PLS-DA[28, 29] were used to

19 screen the differential lipid molecules by combining with fold change and student's t test.

20 **Statistics**

21 All data in this study were expressed as mean ± SEM. Statistical analysis was conducted

22 using the GraphPad Prism 7.0 (GraphPad Software Inc. San Diego, CA) and SPSS 20.0

1   software. To establish statistical significance, student's t-test was used for two-group

2   comparisons and two-way ANOVA followed by Bonferroni's post hoc test used to compare

3   more than two groups. P values< 0.05 were considered statistically significant.

1 **RESULTS**

2 **1. ACSL4 expression is upregulated during kidney fibrosis.**

3 TECs ferroptosis can promote interstitial fibrosis[17], and ACSL4 is an important regulator in

4 the lipid metabolism of ferroptosis[30]. To determine the role of ACSL4 in fibrotic kidneys, we

5 first examined the expression of ACSL4 in wild-type mice under the UUO and FA-treated. By

6 the way of immunofluorescence, we found that ACSL4 was highly expressed in the renal

7 tubules of both two renal fibrosis models (Fig.1a-b). GPX4 is regarded as an essential

8 regulator in ferroptosis. In our results, the protein expressions of ACSL4 and GPX4 were

9 significantly elevated and decreased in the kidney tissues of FA and UUO-induced mice,

10 compared with control groups as well (Fig.1c-d). Then, Nephroseq analysis

11 (https://www.nephroseq.org/resource /login.html) was used to explore the relationship

12 between the mRNA expression of ACSL4 and human renal fibrosis (Fig. 1e) and found that

13 the mRNA value of ACSL4 was shown to be significantly increased in patients with CKD.

14 The patients were divided into three groups according to the classification of clinical

15 manifestation, eGFR. The group of CKD (eGFR less than 60 ml/min, n = 73) has a tight

16 relationship with the increased mRNA value of ACSL4 compared with the group of health

17 control (eGFR more than 90 ml/min, n=63). The results are also shown in Fig. 1e and

18 correlated significantly with GFR levels (r^2=0.2194, p<0.0001, n=186). Overall, these data

19 indicate that ACSL4 was a risk factor for kidney fibrosis.

20 **2. Inhibition of ACSL4 ameliorates kidney intestinal fibrosis by reducing ferroptosis.**

21 To verify the role of ACSL4 in the ferroptosis of kidney fibrosis, we determined whether the

22 inhibition of ACSL4 could abrogate ferroptosis in kidney fibrosis. As a peroxisome

1   proliferator-activated receptor γ (PPARγ) activator, rosiglitazone (ROSI) has a specific

2   inhibitory effect on ACSL4 independently of PPARγ signaling[31]. Our study used UUO and FA

3   mouse models treated with ROSI by intraperitoneal injection and sacrificed on days 14 and 28

4   separately, to determine the role of ACSL4 inhibition in renal fibrosis. The accumulation of

5   lipid peroxide is one hallmark of ferroptosis and 4-HNE is an α, β-unsaturated hydroxyalkenal

6   that is produced by lipid peroxidation in cells. GPX4 can catalyze the reduction of lipid

7   peroxidation in a complex cellular membrane environment[32]. First, in immunofluorescence,

8   we found that ROSI reduced lipid peroxidation in UUO and FA-induced kidney fibrosis, as

9   indicated by the decrease in GPX4 and 4-HNE on renal tubules (Fig. 2a). Subsequently, the

10   protein level expressions of ACSL4, LPCAT3 and GPX4, core proteins in the regulation of

11   ferroptosis, were determined in UUO and FA-induced mice treated with ACSL4 inhibitor

12   ROSI. As shown in Fig. 2b-c, ROSI was also found to downregulate the protein levels of

13   ACSL4 and LPCAT3, and upregulate the expression of the antioxidant GPX4.

14   In addition, the role of ACSL4 was also investigated in ferroptosis of TGF-β-induced fibrotic

15   response. Measurement of reactive oxygen species (ROS) by the lipid ROS probe of C11-

16   BODIPY 581/591 was used to measure lipid peroxidation. ROSI also reduced the high

17   reaction of lipid peroxidation induced in renal fibrosis (fluorescence was shifted from red to

18   green to represent reactive oxygen species) and decreased the expression of 4-HNE in TGF-β-

19   treated cells (Figure 3a), suggesting that ROSI inhibits lipid peroxidation under kidney

20   fibrosis. Consistent with the in vivo results, ROSI also down-regulated the protein level

21   expression of ACSL4 and LPCAT3, which were highly expressed in TGF-β-induced HK-2

22   cells, and effectually rescued GPX4 expression (Fig. 3b). We also found that HK-2 cells

1 treated with TGF-β for 48h induced low cell viability with MTT assay and high cell

2 cytotoxicity with LDH released detection, which can be improved by ACSL4 inhibitor ROSI

3 (Fig.3c-d).

4 In conclusion, our results demonstrated the important role of ACSL4 in the ferroptosis of

5 renal fibrosis and showed that inhibiting ACSL4 may reduce the occurrence of ferroptosis in

6 renal fibrosis.

7 **3. Inhibition of ACSL4 ameliorates kidney intestinal fibrosis by reducing ferroptosis.**

8 Based on the above experimental findings, we speculated whether inhibition of ACSL4

9 alleviates renal fibrosis progression by decreasing ferroptosis. UUO and FA-induced kidneys

10 exhibited severe renal structural damage such as tubulo-interstitial expansion, brush border

11 loss and inflammatory cell infiltration (Fig. 4a). After ROSI-treated, these morphologic

12 abnormalities were ameliorated (Fig. 4a). Additionally, in the UUO and FA mice, MTS

13 showed substantial collagen deposition in the kidney interstitium. However, collagen fiber

14 streaks were reduced after treated mice with ROSI (Fig. 4a). Correspondingly, the protein and

15 mRNA expressions of fibrotic related markers, for instance, fibronectin, collagen-I and α-

16 smooth muscle actin (α-SMA), were also evidently decreased in ROSI-treated mice with

17 fibrotic kidney than those in UUO and FA mice (Fig. 4b-d).

18 Moreover, we have validated the role of ROSI in the kidney fibrotic response in vitro. The

19 results showed that fibronectin and α-SMA were considerably expressed in TGF-β-induced

20 HK-2 cells, and remarkably expressed after ROSI treatment, which were evaluated by

21 immunofluorescence (Fig.5a). Likewise, we detected the expression of the fibrosis markers

22 including fibronectin, collagen-I and α-SMA by immunoblotting and RT-qPCR, and found

1   that the upregulated fibrosis makers were reduced after ROSI treatment in TGF-β-induced

2   HK-2 cell (Fig. 5b-c).

3   In conclusion, these results support a useful effect of ACSL4 inhibition in resisting the TGF-

4   β-induced fibrotic response.

5   **4.   ACSL4 inhibition counteracts TGF-β expression and TGF-β/Smads signaling in**

6   **   TECs.**

7   As a major fibrosis-inducing factor, TGF-β participates in both the fibrosis signaling pathway

8   and induces the secretion of pro-fibrotic factors, which have a profound effect on the

9   evolution of renal fibrosis[8]. To investigate the mechanism by which ACSL4 amplifies fibrosis

10   in the damaged kidney, we detected the expression of the TGF-β/Smads signal pathway by

11   immunoblotting. As shown in Fig. 6a and 6b, inhibiting ACSL4 obviously downregulated the

12   high expression of TGF-β, p-Smad3 as well as p-Smad2 in both UUO and FA-treated kidneys.

13   Meanwhile, we examined the mRNA expression of some profibrotic cytokines, such as TGF-

14   β, connective tissue growth factor (CTGF), fibroblast growth factor 2 (FGF2) and platelet-

15   derived growth factor subunit B (PDGFB), and found that ROSI also attenuated the release of

16   profibrotic cytokines in the fibrotic kidneys with UUO and FA-treated (Fig.6c).

17   In a further step, we performed the validation in the TGF-β-induced TEC fibrosis. The results

18   the same as in vivo showed that the protein level of the TGF-β/Smads signaling pathway

19   (TGF-β, p-Smad3 and p-Smad2) were significantly increased in the TGF-β treated group than

20   in the control and they were reduced in response to ROSI (Fig.7a). Similarly, we observed

21   that the gene level of various profibrotic cytokines (TGF-β, CTGF, FGF2, and PDGFB) were

22   blunted in the TGF-β-induced HK-2 cells after ROSI treatment (Fig.7b)

1   The above data suggest that ACSL4 inhibition may prevent kidney fibrosis by inhibiting

2   TGF-β/Smads signaling pathway and reducing the release of profibrotic factors in TECs.

3   **5.   Knockdown of ACSL4 protects TGF-β-induced TECs from fibrosis by inhibiting**

4   **ferroptosis and reducing profibrotic cytokines.**

5   To further investigate the importance of ACSL4 in kidney fibrosis, we knocked down ACSL4

6   in TECs to verify if it can rescue TGFβ-induced TECs fibrotic reaction in vitro. We

7   transfected ACSL4 siRNA into HK-2 treated with TGF-β and explored the role of ACSL4

8   knockdown in ferroptosis of kidney fibrosis. Lipid peroxidation was shown as the reduced

9   levels of green fluorescence (BODIPY 581/591 C11) and the fluorescence intensity of 4-HNE

10 were decreased by ACSL4 siRNA, which were originally increased in HK-2 cells with TGF-β

11 treatment (Fig. 8a). Then, ACSL4-knockdown induced a rare expression of ferroptosis

12 regulatory proteins (ACSL4 and LPCAT3) and remarkable upregulation of GPX4 in TGF-β-

13 treated HK-2 cells compared to those in control siRNA transfected cells as assayed by

14 immunoblotting (Fig.8b). The results showed that ACSL4 knockdown reduced the release of

15 LDH and improved cell viability determined by the MTT assay (Fig. 8c-d). These results

16 support the above conclusion that high expression of ACSL4 in renal fibrosis which induces

17 ferroptosis in TECs.

18 Subsequently, we explored whether knockdown of ACSL4 could attenuate renal fibrosis via

19 blocking ferroptosis. The results showed that the fibrotic alterations in HK-2 cells under

20 different treatments were detected by immunofluorescence and striking decreases in fibrosis

21 makers (fibronectin and α-SMA) were found in TGF-β-induced HK-2 cells after ACSL4

22 knockdown (Fig.9a). As shown in Fig.9b, the results indicated that the knockdown of ACSL4

20

1 suppressed the expression of the fibrotic makers (fibronectin, collagen-I and α-SMA) in HK-2

2 cells with TGF-β treatment. Following, we examined the mRNA level of fibronectin,

3 collagen-I and α-SMA by RT-qPCR and found that fibrotic makers in TGF-β-induced HK-2

4 cells showed a significantly high level. It can be concluded that ACSL4 siRNA transfection

5 protected HK-2 cells against the progression of fibrotic (Fig.9c).

6 The above data suggest that ACSL4 knockdown may delay the progression of renal fibrosis

7 by aborting ferroptosis.

8 **6. ACSL4 generates ferroptotic precursors by regulate esterification of AA-PE and**

9 **AdA-PE**

10 It has been shown that ACSL4 regulates ferroptosis by specifically esterifying AA and AdA to

11 phospholipids of cell membranes for lipid biosynthesis[24]. We have demonstrated that ACSL4

12 may aggravate kidney fibrosis by promoting ferroptosis and explored how ACSL4 alters the

13 sensitivity to ferroptosis in renal fibrosis by changing the lipid composition of phospholipids

14 of the cell membrane.

15 To validate the expression of ferroptotic precursors phospholipids, we performed lipidomic

16 LC-MS/MS analysis of kidney tissues from UUO mice and ROSI-treated UUO mice. Overall,

17 we detected 102 different types of PE (data not shown) in the fibrotic kidney of mice.

18 Moreover, one study verified that AA-PE and AdA-PE, but not others, were identified as

19 precursors of ferroptotic signals[21]. We observed that C18:0/ C20:4 and C18:0/C22:4 (AA-PE

20 and AdA-PE) were markedly upregulated in UUO mice compared to WT mice and the high

21 level of AA-PE and AdA-PE in UUO mice were markedly reduced after rosiglitazone

22 treatment (Fig10.a-b).

1   Overall, the above results indicate that ACSL4 inhibition in kidney fibrosis is accompanied by

2   a reduction of ferroptotic precursors AA-PE and AdA-PE which are utilized as substrates in

3   lipid peroxidation to reduce the ferroptosis cascade reaction.

DISCUSSION

Accumulating studies have found that ferroptosis contributes to numerous diseases, such as AKI and CKD[18, 33, 34, 35]. However, the precise mechanisms of ferroptosis mediate fibrotic kidney still require further elucidation, our study emphasizes the importance of ACSL4 in this process. Findings from our study revealed that ACSL4, as the lynchpin in the reprogramming of lipid metabolism, aggravates renal fibrosis by activating endogenous ferroptotic mechanisms. In previous studies, it was found that renal tubular epithelial cell death, such as necroptosis and pyroptosis, participated in the pathogenesis of renal fibrosis. In this study, we found that the fibrotic kidney diseases, both in UUO/FA-induced mouse model and the TGF-β-induced HK-2 cell model, were associated with increased ferroptosis and upregulation of ACSL4. From this, we inferred that ferroptosis of TECs may be one of the potential mechanisms of renal fibrosis, and inhibition of ferroptosis by targeting ACSL4 may be an effective treatment for alleviating renal fibrosis.

ACSL4 is the enzyme of the long-chain acyl coenzyme A synthase family, which regulates lipid biosynthesis by activating PUFAs[36]. As the main substrates of lipids peroxidation in ferroptosis, PUFAs are susceptible to undergoing oxidation and produced hydroperoxides of PUFAs (PUFA-OOH)[37]. It is necessary for the execution of ferroptosis and which can be enhanced by ACSL4. ACSL4 also promotes PE of membrane production by esterifying PUFAs to PUFA-coA, thereby participating in the occurrence of lipid metabolism reprogramming in ferroptosis[24] ACSL4 is the crucial regulator to mediate ferroptosis through the reprogramming of lipid metabolism[24, 38] and participates in the pathological process of various diseases under intensity, heart, lung and muscel[21, 25, 26, 39, 40, 41]. Recent studies have

23

1 found that ACSL4-mediated ferroptosis is also implicated in kidney disease[42, 43, 44]. Wang et

2 al. demonstrated that ACSL4 plays a protector in the ferroptosis of AKI by knocking out

3 ACSL4 in TECs of mice[43]. In human acute tubular injury, the expression of ACSL4 in TECs

4 is upregulated, accomplished with the elevation of serum creatinine and blood urea nitrogen

5 and the declined level of eGFR[45]. Muller et al. and Yuan et al. suggested that the expression of

6 ACSL4 can be served as a biomarker to help predict the relationship between ferroptosis and

7 the pathological mechanism of disease[42, 46]. The findings of Wang[18] and Zhou[30] indicated that

8 the execution of ferroptosis can aggravate the progression of CKD. The kidney is also

9 regarded as an important site that actively participates in the systemic regulation of lipid

10 metabolism. Thus, we found that ACSL4 is upregulated in the kidney tissue of CKD through

11 the analysis of the Nephroseq-database and the experiments of renal fibrosis in vivo and vitro,

12 and is also involved in the ferroptosis-related fibrotic kidney. These results indicate that

13 ACSL4 is a crucial inducer in the ferroptosis of renal fibrosis.

14 Cell death and EMT caused by injured TECs are the key triggers in renal fibrosis[17, 47]. TGF-

15 β/Smads signaling was demonstrated as the activation that induced EMT phenotypes in

16 TECs[9, 48]. TGF-β is one of the most critical profibrotic cytokine which stimulates the secretion

17 of profibrogenic cytokines, such as CTGF, FGF2 and PDGFB. To explore whether ACSL4

18 aggravated renal fibrosis by the TGF-β/Smads signaling and the variety of profibrotic factors,

19 ACSL4 inhibitor ROSI was treated in TGF-β-induced TECs and mouse models. We found

20 that inhibition of ACSL4 by ROSI alleviated the fibrotic TECs and reduced the creation of

21 profibrotic factors by abolishing ferroptosis. A study from randomized clinical trials indicates

22 that ROSI as a peroxisome proliferator-activated receptor γ (PPARγ) agonist has favorable

1   effects on renal disease progression[49]. Due to the specific inhibitory effect on ACSL4, ROSI

2   can affect ferroptosis independently of PPARγ[50]. The results in the cells by ACSL4

3   knockdown were the same as the ROSI inhibition. Thus, we suggested that the suppression of

4   ACSL4 alleviates renal fibrosis by inhibiting ferroptosis rather than stimulating PPARγ.

5   These results indicate that ACSL4 is a crucial factor that accelerates the progression of renal

6   fibrosis through activating TGF-β/Smad signal pathway and releasing several profibrotic

7   factors.

8   Excessive PUFAs are prone to induce lipid peroxidation and also are a risk factor in patients

9   with CKD. GPX4 is the crucial antioxidant that controls ferroptosis and alleviates lipid

10   hydroperoxides within biological membranes, and its decrease can be caused by the

11   dysregulation of the redox system caused by the high expression of ACSL4[31]. We validated

12   this solution at the pharmacological and genetic levels and found that inhibition of ACSL4

13   can reduce lipid peroxidation, thereby elevating the expression of GPX4. AA and AdA in

14   PUFAs are more sensitive to lipid peroxidation, which can be preferentially acylated by

15   ACSL4 and then participate in the synthesis of phosphatidylethanolamine under the action of

16   LPCAT3, and the product becomes the important ferroptotic signals[38, 51]. Mao et al. analyzed

17   the Redox phospholipidomics in Gpx4-deficient mouse embryonic fibroblasts by LC-MS/MS

18   identification and found that PE molecular species with C18:0 fatty acids and C20:4 (AA) or

19   C22:4 (AdA) fatty acids were decreased in ACSL4 KO cells[24]. By lipidomic analysis, our

20   study also showed that the expressions of AA-PE (C18:0/C20:4) and AdA-PE (C18:0/C22:4)

21   were decreased after ROSI treatment in UUO. Therefore, we suggest that renal fibrosis may

22   be caused by ACSL4-induced incrassation of AA-PE and AdA-PE in membrane

phospholipids which are the ferroptotic precursors. The results demonstrated that ACSL4 is

involved in the esterified oxidated PUFAs in fibrotic kidney and highlighted the importance

of inhibiting ACSL4 as a blocker of ferroptotic lipid signaling which provides new

pharmacological targets.

CONCLUSION

In conclusion, our present findings demonstrate that ACSL4 activation during kidney fibrosis

development contributes to tubular ferroptosis, and inhibition of ferroptosis by targeting

ACSL4 rescue chronic kidney injury. Identifying the PUFAs especially AA and AdA, which

are modulated by ACSL4, may provide new insights into understanding the signalling

pathway involved in ferroptosis of TECs during kidney fibrosis. The protective effects to treat

ferroptotic TECs in CKD deserve further exploration and will develop more novel therapeutic

approaches for CKD.

11 **Data availability statement**

12 The data that support the findings of this study are available from the corresponding author

13 upon reasonable request.

14

15 **Ethics statement**

16 This paper does not describe studies involving human participants, human data or human

17 tissue. All animal interventions were approved by the Institutional Animal Care and Use

18 Committee Tongji Medical College, Huazhong University of Science and Technology, China

19 (No. S 2670).

20

21 **Conflict to interest**

22 The authors declare that there is no conflict of interest.

1

Author contributions

2

Y.D. performed the experiment-related validation and investigation, data analysis and original

3

draft writing. Y.T.C. participated in the research design and provided methodology. D.X.M.M.

4

provided critical suggestions in this study. R.J. reviewed the manuscript. Y.H. and L.Z.

5

supervised experiments. C.T.Z. contributed to analytic tools. H.Y.G administrated this project

6

and reviewed the manuscript. Q.Y. participated in the research conception and design, project

7

administration and manuscript-revised.

8

References:

1. Glassock RJ, Warnock DG, Delanaye P. The global burden of chronic kidney disease: estimates, variability and pitfalls. *Nat Rev Nephrol* 2017, **13**(2): 104-114.

2. Webster AC, Nagler EV, Morton RL, Masson P. Chronic Kidney Disease. *The Lancet* 2017, **389**(10075): 1238-1252.

3. Eddy AA. Overview of the cellular and molecular basis of kidney fibrosis. *Kidney Int Suppl (2011)* 2014, **4**(1): 2-8.

4. Venkatachalam MA, Weinberg JM, Kriz W, Bidani AK. Failed Tubule Recovery, AKI-CKD Transition, and Kidney Disease Progression. *J Am Soc Nephrol* 2015, **26**(8): 1765-1776.

5. Venkatachalam MA, Griffin KA, Lan R, Geng H, Saikumar P, Bidani AK. Acute kidney injury: a springboard for progression in chronic kidney disease. *Am J Physiol Renal Physiol* 2010, **298**(5): F1078-1094.

6. Liu BC, Tang TT, Lv LL. How Tubular Epithelial Cell Injury Contributes to Renal Fibrosis. *Adv Exp Med Biol* 2019, **1165:** 233-252.

7. Qi R, Yang C. Renal tubular epithelial cells: the neglected mediator of tubulointerstitial fibrosis after injury. *Cell Death Dis* 2018, **9**(11): 1126.

8. Kaissling B, Lehir M, Kriz W. Renal epithelial injury and fibrosis. *Biochimica et biophysica acta* 2013, **1832**(7): 931-939.

9. Lovisa S, Zeisberg M, Kalluri R. Partial Epithelial-to-Mesenchymal Transition and Other New Mechanisms of Kidney Fibrosis. *Trends Endocrinol Metab* 2016, **27**(10): 681-695.

10. Chevalier RL. Growth factors and apoptosis in neonatal ureteral obstruction. *J Am Soc Nephrol* 1996, **7**(8): 1098-1105.

11. Shi Y, Chen X, Huang C, Pollock C. RIPK3: A New Player in Renal Fibrosis. *Frontiers in Cell and Developmental Biology* 2020, **8**.

12. Maremonti F, Meyer C, Linkermann A. Mechanisms and Models of Kidney Tubular Necrosis and Nephron Loss. *J Am Soc Nephrol* 2022.

13. Priante G, Gianesello L, Ceol M, Del Prete D, Anglani F. Cell Death in the Kidney. *International journal of molecular sciences* 2019, **20**(14).

14. Dixon SJ, Lemberg KM, Lamprecht MR, Skouta R, Zaitsev EM, Gleason CE*, et al.* Ferroptosis: an iron-dependent form of nonapoptotic cell death. *Cell* 2012, **149**(5): 1060-1072.

15. Zhang J, Bi J, Ren Y, Du Z, Li T, Wang T*, et al.* Involvement of GPX4 in irisin's protection against ischemia reperfusion-induced acute kidney injury. *J Cell Physiol* 2021, **236**(2): 931-945.

16. Li D, Liu B, Fan Y, Liu M, Han B, Meng Y*, et al.* Nuciferine protects against folic acid-induced acute kidney injury by inhibiting ferroptosis. *British journal of pharmacology* 2021, **178**(5): 1182-1199.

17. Zhou L, Xue X, Hou Q, Dai C. Targeting Ferroptosis Attenuates Interstitial Inflammation and Kidney Fibrosis. *Kidney Diseases* 2021: 1-15.

18. Wang J, Wang Y, Liu Y, Cai X, Huang X, Fu W*, et al.* Ferroptosis, a new target for treatment of renal injury and fibrosis in a 5/6 nephrectomy-induced CKD rat model. *Cell death discovery* 2022, **8**(1): 127.

19. Zhang B, Chen X, Ru F, Gan Y, Li B, Xia W*, et al.* Liproxstatin-1 attenuates unilateral

ureteral obstruction-induced renal fibrosis by inhibiting renal tubular epithelial cells ferroptosis. *Cell Death Dis* 2021, **12**(9): 843.

20. Forcina GC, Dixon SJ. GPX4 at the Crossroads of Lipid Homeostasis and Ferroptosis. *Proteomics* 2019, **19**(18): e1800311.

21. Kagan VE, Mao G, Qu F, Angeli JP, Doll S, Croix CS, *et al.* Oxidized arachidonic and adrenic PEs navigate cells to ferroptosis. *Nature chemical biology* 2017, **13**(1): 81-90.

22. Liang A, Wang Y, Woodard LE, Wilson MH, Sharma R, Awasthi YC, *et al.* Loss of glutathione S-transferase A4 accelerates obstruction-induced tubule damage and renal fibrosis. *J Pathol* 2012, **228**(4): 448-458.

23. Dixon SJ, Winter GE, Musavi LS, Lee ED, Snijder B, Rebsamen M, *et al.* Human Haploid Cell Genetics Reveals Roles for Lipid Metabolism Genes in Nonapoptotic Cell Death. *ACS Chem Biol* 2015, **10**(7): 1604-1609.

24. Doll S, Proneth B, Tyurina YY, Panzilius E, Kobayashi S, Ingold I, *et al.* ACSL4 dictates ferroptosis sensitivity by shaping cellular lipid composition. *Nature chemical biology* 2017, **13**(1): 91-98.

25. Li Y, Feng D, Wang Z, Zhao Y, Sun R, Tian D, *et al.* Ischemia-induced ACSL4 activation contributes to ferroptosis-mediated tissue injury in intestinal ischemia/reperfusion. *Cell Death Differ* 2019, **26**(11): 2284-2299.

26. Xu Y, Li X, Cheng Y, Yang M, Wang R. Inhibition of ACSL4 attenuates ferroptotic damage after pulmonary ischemia-reperfusion. *FASEB J* 2020, **34**(12): 16262-16275.

27. Chauhan MZ, Valencia AK, Piqueras MC, Enriquez-Algeciras M, Bhattacharya SK. Optic Nerve Lipidomics Reveal Impaired Glucosylsphingosine Lipids Pathway in Glaucoma. *Invest Ophthalmol Vis Sci* 2019, **60**(5): 1789-1798.

28. Barker M, Rayens W. Partial least squares for discrimination. *Journal of Chemometrics* 2003, **17**(3): 166-173.

29. Westerhuis JA, Hoefsloot HCJ, Smit S, Vis DJ, Smilde AK, van Velzen EJJ, *et al.* Assessment of PLSDA cross validation. *Metabolomics* 2008, **4**(1): 81-89.

30. Yuan H, Li X, Zhang X, Kang R, Tang D. Identification of ACSL4 as a biomarker and contributor of ferroptosis. *Biochemical and biophysical research communications* 2016, **478**(3): 1338-1343.

31. Askari B, Kanter JE, Sherrid AM, Golej DL, Bender AT, Liu J, *et al.* Rosiglitazone inhibits acyl-CoA synthetase activity and fatty acid partitioning to diacylglycerol and triacylglycerol via a peroxisome proliferator-activated receptor-gamma-independent mechanism in human arterial smooth muscle cells and macrophages. *Diabetes* 2007, **56**(4): 1143-1152.

32. Yang WS, SriRamaratnam R, Welsch ME, Shimada K, Skouta R, Viswanathan VS, *et al.* Regulation of ferroptotic cancer cell death by GPX4. *Cell* 2014, **156**(1-2): 317-331.

33. Yang L, Guo J, Yu N, Liu Y, Song H, Niu J, *et al.* Tocilizumab mimotope alleviates kidney injury and fibrosis by inhibiting IL-6 signaling and ferroptosis in UUO model. *Life sciences* 2020, **261**: 118487.

34. Friedmann Angeli JP, Schneider M, Proneth B, Tyurina YY, Tyurin VA, Hammond VJ, *et al.* Inactivation of the ferroptosis regulator Gpx4 triggers acute renal failure in mice. *Nat Cell Biol* 2014, **16**(12): 1180-1191.

35. Linkermann A, Skouta R, Himmerkus N, Mulay SR, Dewitz C, De Zen F, *et al.*

1   Synchronized renal tubular cell death involves ferroptosis. *Proceedings of the National*
2   *Academy of Sciences of the United States of America* 2014, **111**(47)**:** 16836-16841.

3   36.   Belavgeni A, Meyer C, Stumpf J, Hugo C, Linkermann A. Ferroptosis and Necroptosis in
4   the Kidney. *Cell Chem Biol* 2020, **27**(4)**:** 448-462.

5   37.   Yang WS, Kim KJ, Gaschler MM, Patel M, Shchepinov MS, Stockwell BR. Peroxidation of
6   polyunsaturated fatty acids by lipoxygenases drives ferroptosis. *Proceedings of the*
7   *National Academy of Sciences of the United States of America* 2016, **113**(34)**:** E4966-
8   4975.

9   38.   Cheng J, Fan YQ, Liu BH, Zhou H, Wang JM, Chen QX. ACSL4 suppresses glioma cells
10   proliferation via activating ferroptosis. *Oncol Rep* 2020, **43**(1)**:** 147-158.

11   39.   Cui Y, Zhang Y, Zhao X, Shao L, Liu G, Sun C, *et al.* ACSL4 exacerbates ischemic stroke
12   by promoting ferroptosis-induced brain injury and neuroinflammation. *Brain Behav*
13   *Immun* 2021, **93:** 312-321.

14   40.   Tuo QZ, Liu Y, Xiang Z, Yan HF, Zou T, Shu Y, *et al.* Thrombin induces ACSL4-dependent
15   ferroptosis during cerebral ischemia/reperfusion. *Signal Transduct Target Ther* 2022,
16   **7**(1)**:** 59.

17   41.   He S, Li R, Peng Y, Wang Z, Huang J, Meng H, *et al.* ACSL4 contributes to ferroptosis-
18   mediated rhabdomyolysis in exertional heat stroke. *J Cachexia Sarcopenia Muscle* 2022.

19   42.   Pei Z, Liu Y, Liu S, Jin W, Luo Y, Sun M, *et al.* FUNDC1 insufficiency sensitizes high fat diet
20   intake-induced cardiac remodeling and contractile anomaly through ACSL4-mediated
21   ferroptosis. *Metabolism* 2021, **122:** 154840.

22   43.   Müller T, Dewitz C, Schmitz J, Schröder AS, Bräsen JH, Stockwell BR, *et al.* Necroptosis
23   and ferroptosis are alternative cell death pathways that operate in acute kidney failure.
24   *Cellular and molecular life sciences : CMLS* 2017, **74**(19)**:** 3631-3645.

25   44.   Wang Y, Zhang M, Bi R, Su Y, Quan F, Lin Y, *et al.* ACSL4 deficiency confers protection
26   against ferroptosis-mediated acute kidney injury. *Redox Biol* 2022, **51:** 102262.

27   45.   Kuwata H, Tomitsuka Y, Yoda E, Hara S. Role of ACSL4 in the chemical-induced cell
28   death in human proximal tubule epithelial HK-2 cells. *Biosci Rep* 2022, **42**(2).

29   46.   Zhao Z, Wu J, Xu H, Zhou C, Han B, Zhu H, *et al.* XJB-5-131 inhibited ferroptosis in
30   tubular epithelial cells after ischemia-reperfusion injury. *Cell Death Dis* 2020, **11**(8)**:** 629.

31   47.   Humphreys BD. Mechanisms of Renal Fibrosis. *Annu Rev Physiol* 2018, **80:** 309-326.

32   48.   Meng XM, Nikolic-Paterson DJ, Lan HY. TGF-beta: the master regulator of fibrosis. *Nat*
33   *Rev Nephrol* 2016, **12**(6)**:** 325-338.

34   49.   Bottinger EP, Bitzer M. TGF-beta signaling in renal disease. *J Am Soc Nephrol* 2002,
35   **13**(10)**:** 2600-2610.

36   50.   Bolignano D, Zoccali C. Glitazones in chronic kidney disease: potential and concerns.
37   *Nutr Metab Cardiovasc Dis* 2012, **22**(3)**:** 167-175.

38   51.   Brigelius-Flohé R, Maiorino M. Glutathione peroxidases. *Biochimica et biophysica acta*
39   2013, **1830**(5)**:** 3289-3303.

40

1   **Figure legend**

2   **FIGURE 1 Expression of ACSL4 in fibrotic kidney.** (a, b) The representative images (six

3   visual fields for each sample analyzed) of immunofluorescence staining of ACSL4 in UUO and

4   FA-induced kidney sections from indicated groups (left panel). Quantitative images to depict

5   fluorescence intensity (Right panel). Scale bars: 50 μm. $n = 3$ mice. (c) Western-blot analysis of

6   ACSL4 and GPX4 in UUO-treated mice separately (right panel). Schematic representation of

7   quantitative data of indicated proteins. Representative images from three independent experiments

8   are shown above. n = 3 mice. (d) Western-blot analysis of ACSL4 and GPX4 in FA-treated mice

9   separately (right panel). Schematic representation of quantitative data of indicated proteins.

10   Representative images from three independent experiments are shown above. $n = 3$ mice. (e) A

11   negative correlation between tubular ACSL4 and eGFR was observed in the public Nephroseq

12   dataset. Data are presented as mean ± SEM. *$P < 0.05$, ns means no statistical significance.

13   **FIGURE 2 Inhibiting ACSL4 reduced TECs ferroptosis in vivo.** (a) The representative

14   image (six visual fields for each sample analyzed) of immunofluorescence staining of 4-HNE and

15   immunohistochemistry staining of GPX4 in kidney sections under indicated conditions.

16   Quantitative images to depict expression intensity are shown down below. Scale bars：50 μm.

17     $n = 5$ mice. (b) Western-blot analyzing the expression of ferroptosis-related proteins (ACSL4,

18   LPCAT3 and GPX4) in the UUO-treated kidney samples (left panel). The relative abundances of

19   the indicated protein expressions were normalized by GAPDH (right panel). $n = 5$ mice. (c)

20   Western-blot analysis of ACSL4, LPCAT3 and GPX4 in FA-treated mice.-Representative images

21   from more than three independent experiments are shown in above and quantitative images are

22   shown in the right panel. n=5 mice. Data are presented as mean ± SEM. *$P < 0.05$, ns means no

1   statistical significance.

2   **FIGURE 3 The relationship between ACSl4 inhibition and TECs ferroptosis in vitro.** (a)

3   Control and TGF-β-induced cells treated with 100 μM ROSI for 48 h were labeled with

4   BODIPY 581/591 C11 and immunofluorescence stained with 4-HNE. Quantitative images to

5   depict fluorescence intensity at the right panel. Scale bar = 50 μm. (b) Western-blot analysis of

6   ACSL4, LPCAT3 and GPX4 in TGF-β-induced HK-2 cells. Representative images from three

7   independent experiments are shown above. Schematic representation of quantitative data of

8   indicated proteins (right panel). (c, d) Cell viability measured via MTT and cell cytotoxicity

9   assayed via LDH revealed a significant change in the death of cultured HK-2 cells in different

10   groups. These data are calculated from more than three independent experiments. Data are

11   presented as mean ± SEM. *$P < 0.05$, ns means no statistical significance.

12   **FIGURE 4 Fibrotic kidney was significantly ameliorated in UUO kidneys after**

13   **inhibiting ACSL4.** (a) The representative image (six visual fields for each sample analyzed)

14   stained with HE, PAS and MTS of kidney sections from UUO, FA or sham-operated kidneys

15   (control). Animals received ACSL4 inhibitor or vehicle as indicated. The tubular lesion and

16   interstitial fibrosis were further presented in quantification. Scale Bar: 50 μm. $n = 5$ mice. (b)

17   Western-blot of UUO-treated whole-kidney lysates analyzing the expression of fibronectin,

18   collagen-I and α-SMA. Schematic representations of quantitative data of indicated proteins shown

19   at the right panel. n=5 mice (c) Western blot analyzing the expression of indicated proteins in

20   the FA-treated kidney samples. The relative abundance of the indicated protein expression

21   was normalized by GAPDH (right panel). **n**=5 mice. (d) The mRNA expression of fibronectin,

22   collagen-111 and a-SMA were analyzed by RT-qPCR in UUO and FA-treated kidneys.

1   Representative images from three independent experiments are shown above. *n*=5 mice.

2   These data are calculated from more than three independent experiments. Data are presented

3   as mean ± SEM. **P* < 0.05, ns means no statistical significance.

4   **FIGURE 5 ACSL4 inhibition improved the fibrosis reaction in TGF-β-induced HK-2**

5   **cells.**(a) The representative images (six visual fields for each sample analyzed) of

6   immunofluorescence staining for fibronectin and α-SMA (green) in the indicated group. The

7   positive areas of indicated protein were further presented in quantification. Scale bars: 50 μm.

8   (b) Western-blot analyzing the expression of fibronectin, collagen-I and α-SMA in the TGF-β-

9   induced HK-2 cells treated with or without ROSI (left panel). GAPDH sets as a loading

10   control. Schematic representation of band intensity of indicated proteins (right panel). (c) RT-

11   qPCR for fibronectin, collagen-I and α-SMA transcripts in total RNA extracts of HK-2 cells

12   with DMSO- or ROSI-treated normal and TGF-β-treated cells. The data were calculated from

13   three independent experiments and expressed as the mean ± SEM. Representative images

14   from more than three independent experiments are shown above. Data are presented as mean

15   ± SEM. **P* < 0.05, ns means no statistical significance.

16   **FIGURE 6 The release of profibrotic cytokines was significantly reduced in UUO and**

17   **FA kidneys after inhibiting ACSL4.** (a, b) Western-blot analyzing the expression of profibrotic

18   cytokines TGF-β, p-Smad2 and p-Smad3 in UUO-and FA-treated kidney samples. The relative

19   abundance of the indicated protein expression was normalized by GAPDH (right panel). *n*=5

20   mice. (c) Profibrotic cytokines TGF-β, CTGF, FGF2 and PDGFB mRNA detected by RT-qPCR

21   analysis in UUO and FA-treated mice. *n*=5 mice. Representative images from more than three

22   independent experiments are shown above. Data are presented as mean ± SEM. **P* < 0.05, ns

means no statistical significance.

FIGURE 7 ACSL4 inhibition reduced profibrotic reaction in TGF-β-induced HK-2 cells.

(a) Western-blot analyzing the expression of profibrotic cytokines TGF-β, p-Smad2 and p-Smad3 in TGF-β-induce HK-2 cells. The relative abundance of the indicated protein expression was normalized by GAPDH. Schematic representation of quantitative data of indicated proteins (right panel). (b) The expressions of profibrotic cytokines TGF-β, CTGF, FGF2 and PDGFB mRNA were analyzed by RT-qPCR in TGF-β-induced HK-2 cells. Representative images from more than three independent experiments are shown above. Data are presented as mean ± SEM. *$P < 0.05$, ns means no statistical significance.

FIGURE 8 The knockdown of ACSL4 reduced TECs ferroptosis. (a)TGF-β-induced HK-2 cells treated with ROSI or DMSO were labeled with BODIPY 581/591 C11 and immunofluorescence stained with 4-HNE. Quantitative images to depict fluorescence intensity at the right panel. Scale bar = 50 μm. (b) Western-blot analysis of ACSL4, LPCAT3 and GPX4 in TGF-β-induced HK-2 cells. Schematic representation of quantitative data of indicated proteins (right panel). Representative images from three independent experiments are shown above. *n*=5 mice. (c, d) Cell viability and cell cytotoxicity were assayed by MTT and LDH respectively. Both demonstrated a significant change in TGF-β-induced HK-2 cells with the knockdown of ACSL4. Representative images from more than three independent experiments are shown above. Data are presented as mean ± SEM. *$P < 0.05$, ns means no statistical significance.

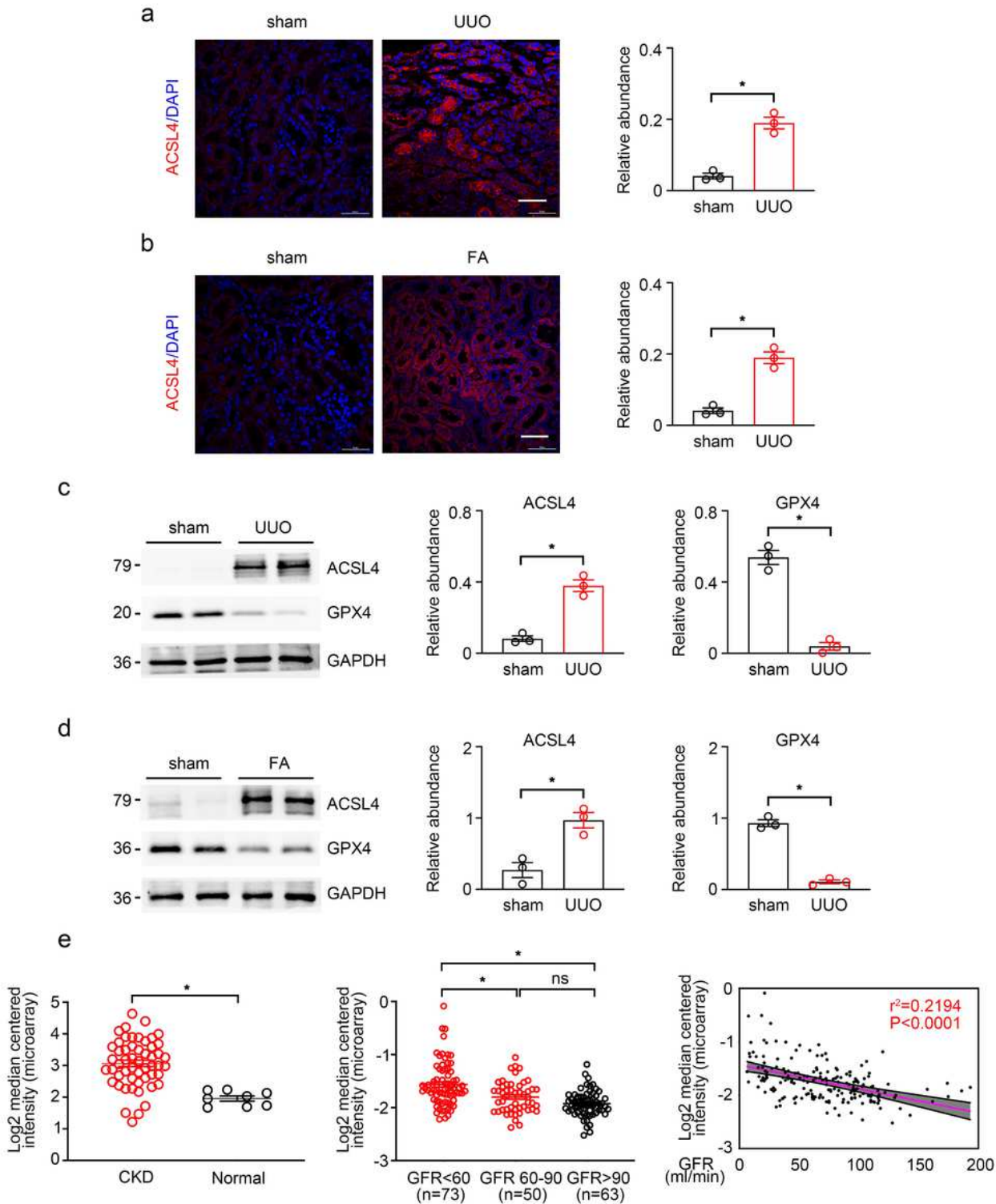**FIGURE 9 Knock ACSL4 down alleviated the progression of kidney fibrosis.** (a)The representative image (six visual fields for each sample analyzed) of immunofluorescence staining for fibronectin and a-SMA (green) in the indicated group of HK-2 cells. The positive areas of

1   indicated protein were further presented in quantification (right panel). (b)Western-blot analyzing

2   the expression of fibronectin, collagen-I and α-SMA in the TGFβ-induced HK-2 cells with or

3   without the knockdown of ACSL4 (right panel). GAPDH sets as the loading control. Schematic

4   representation of band intensity of indicated proteins (left panel). (g) The expression of fibronectin,

5   collagen-I and α-SMA detected by RT-qPCR in TGF-β-induced HK-2 cells with or without the

6   knockdown of ACSL4. Representative images from more than three independent experiments are

7   shown above. Data are presented as mean ± SEM. *$P < 0.05$, ns means no statistical significance.

8   **FIGURE 10 ACSL4 knockdown inhibited the PE ferroptotic precursors in kidney fibrosis**

9   **response.** (a) Quantitative assessment of PE molecular species (C18:0/C20:4 and C18:0/C22:4) in

10   UUO kidney treated with ROSI. Data are presented as mean ± SEM. $n = 6$ mice. (b) Levels of

11   AA-PE and AdA-PE in UUO kidney with or without ROSI. $n = 6$ mice. Data are presented as mean

12   ± SEM. *$P < 0.05$, ns means no statistical significance.

Figures

Figure 1

Expression of ACSL4 in fibrotic kidney. (a, b) The representative images (six visual fields for each sample analyzed) of immunofluorescence staining of ACSL4 in UUO and FA-induced kidney sections from indicated groups (left panel). Quantitative images to depict fluorescence intensity (Right panel). Scale

bars: 50 μm. n = 3 mice. (c) Western-blot analysis of ACSL4 and GPX4 in UUO-treated mice separately (right panel). Schematic representation of quantitative data of indicated proteins. Representative images from three independent experiments are shown above. n = 3 mice. (d) Western-blot analysis of ACSL4 and GPX4 in FA-treated mice separately (right panel). Schematic representation of quantitative data of indicated proteins. Representative images from three independent experiments are shown above. n = 3 mice. (e) A negative correlation between tubular ACSL4 and eGFR was observed in the public Nephroseq dataset. Data are presented as mean ± SEM. *P 0.05, ns means no statistical significance.
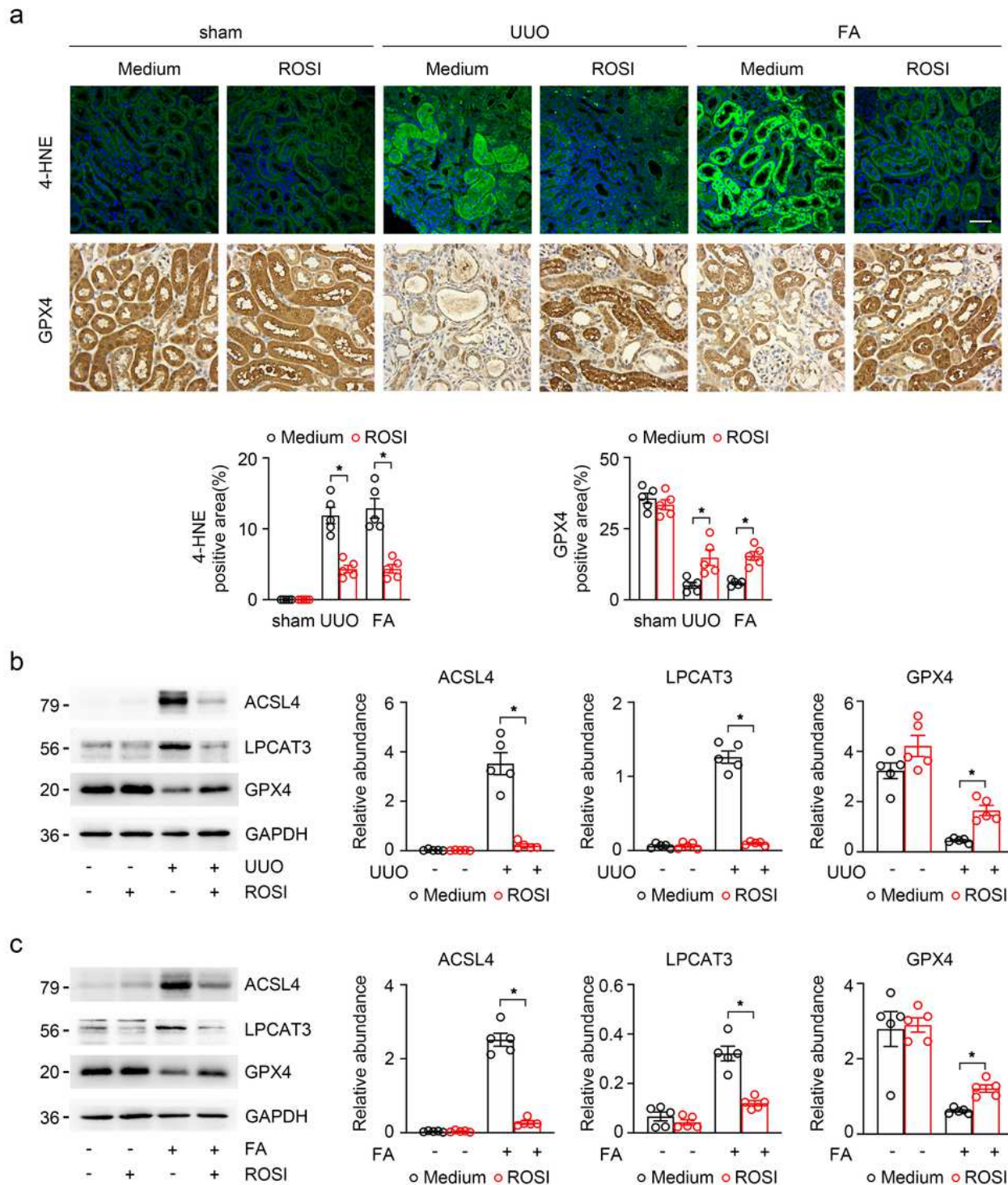
Figure 2

Inhibiting ACSL4 reduced TECs ferroptosis in vivo. (a) The representative image (six visual fields for each sample analyzed) of immunofluorescence staining of 4-HNE and immunohistochemistry staining of GPX4 in kidney sections under indicated conditions. Quantitative images to depict expression intensity are shown down below. Scale bars 50 μm. n = 5 mice. (b) Western-blot analyzing the expression of ferroptosis-related proteins (ACSL4, LPCAT3 and GPX4) in the UUO-treated kidney samples (left panel). The relative abundances of the indicated protein expressions were normalized by GAPDH (right panel). n = 5 mice. (c) Western-blot analysis of ACSL4, LPCAT3 and GPX4 in FA-treated mice. Representative images from more than three independent experiments are shown in above and quantitative images are shown in the right panel. n=5 mice. Data are presented as mean ± SEM. *P 0.05, ns means no statistical significance.
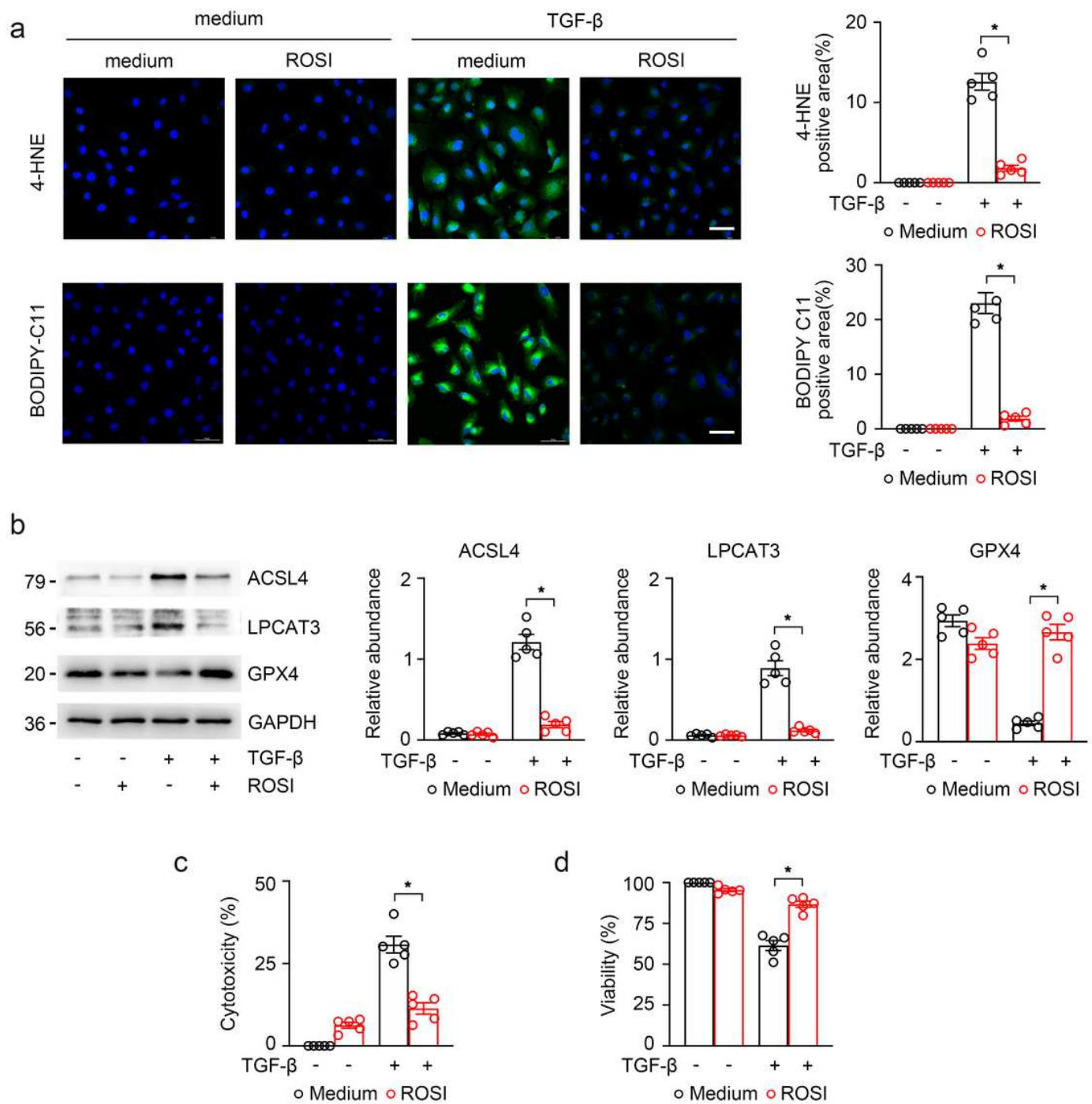
Figure 3

The relationship between ACSl4 inhibition and TECs ferroptosis in vitro. (a) Control and TGF-β-induced cells treated with 100 μM ROSI for 48 h were labeled with BODIPY 581/591 C11 and immunofluorescence stained with 4-HNE. Quantitative images to depict fluorescence intensity at the right panel. Scale bar = 50 μm. (b) Western-blot analysis of ACSL4, LPCAT3 and GPX4 in TGF-β-induced HK-2 cells. Representative images from three independent experiments are shown above. Schematic representation of quantitative data of indicated proteins (right panel). (c, d) Cell viability measured via MTT and cell cytotoxicity

assayed via LDH revealed a significant change in the death of cultured HK-2 cells in different groups. These data are calculated from more than three independent experiments. Data are presented as mean ± SEM. *P 0.05, ns means no statistical significance.
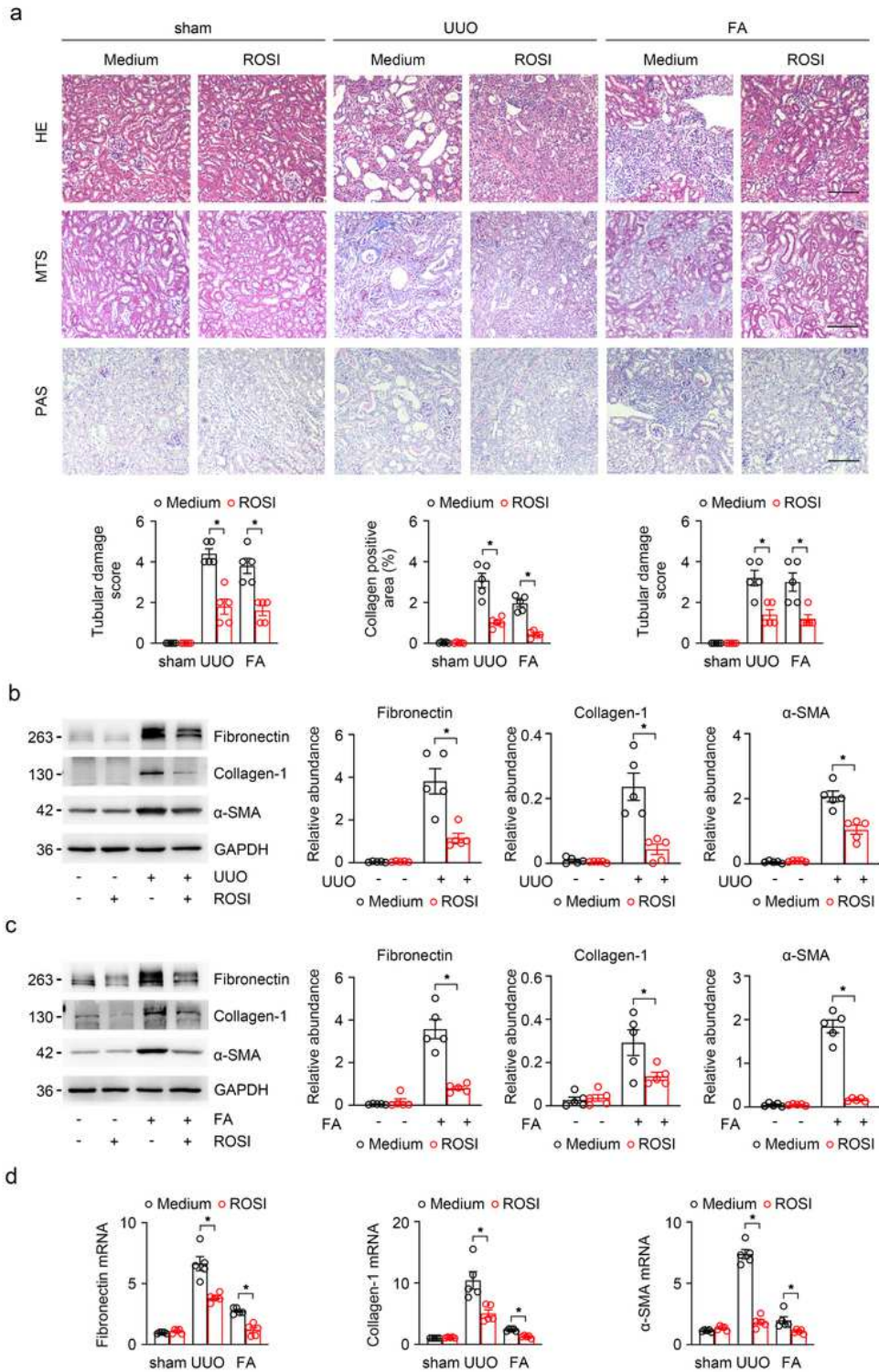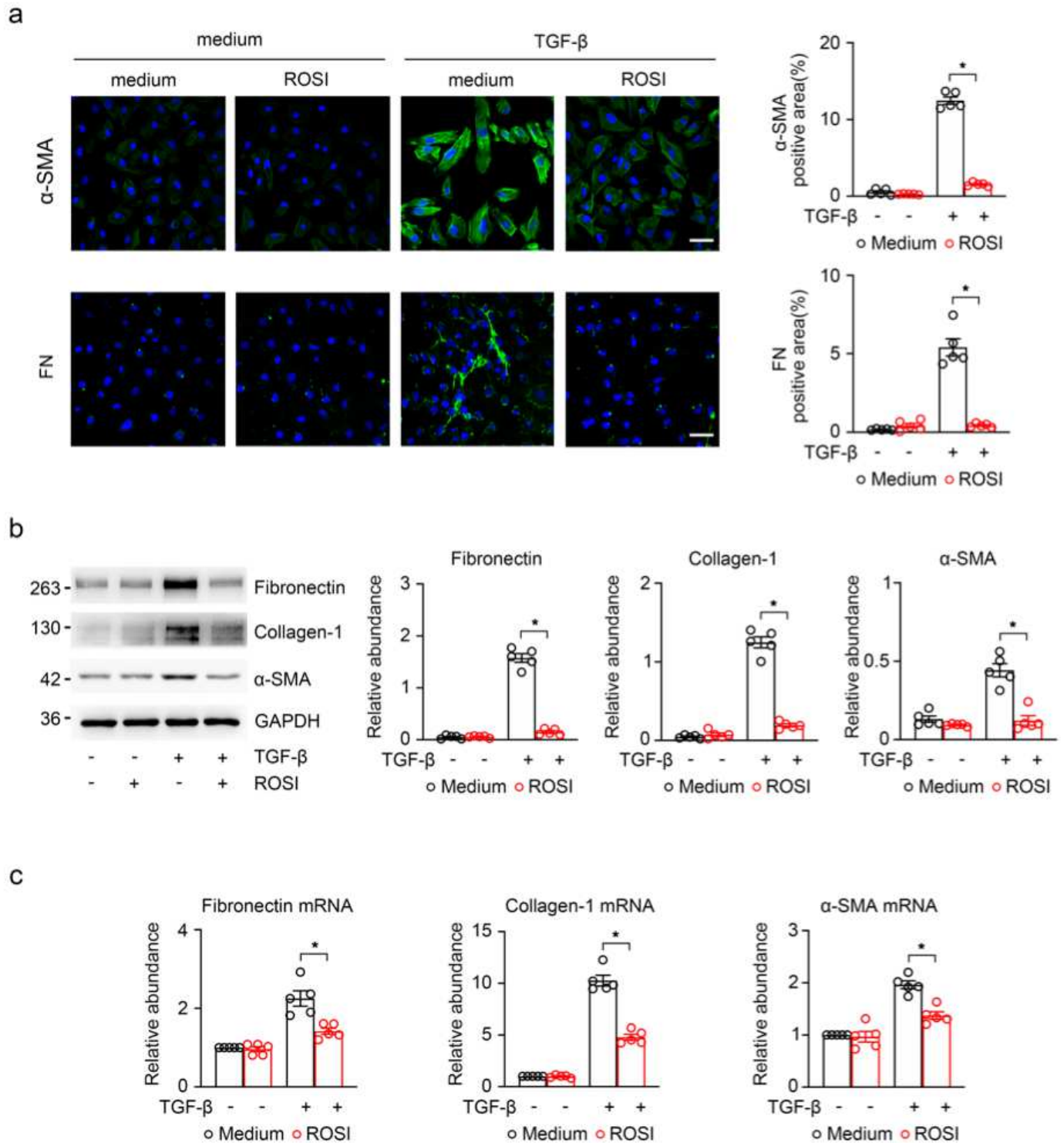

Figure 4

Fibrotic kidney was significantly ameliorated in UUO kidneys after inhibiting ACSL4. (a) The representative image (six visual fields for each sample analyzed) stained with HE, PAS and MTS of kidney sections from UUO, FA or sham-operated kidneys (control). Animals received ACSL4 inhibitor or vehicle as indicated. The tubular lesion and interstitial fibrosis were further presented in quantification. Scale Bar: 50 μm. n = 5 mice. (b) Western-blot of UUO-treated whole-kidney lysates analyzing the expression of fibronectin, collagen-I and α-SMA. Schematic representations of quantitative data of indicated proteins shown at the right panel. n=5 mice (c) Western blot analyzing the expression of indicated proteins in the FA-treated kidney samples. The relative abundance of the indicated protein expression was normalized by GAPDH (right panel). n=5 mice. (d) The mRNA expression of fibronectin, collagen-111 and a-SMA were analyzed by RT-qPCR in UUO and FA-treated kidneys. Representative images from three independent experiments are shown above. n=5 mice. These data are calculated from more than three independent experiments. Data are presented as mean ± SEM. *P 0.05, ns means no statistical significance.
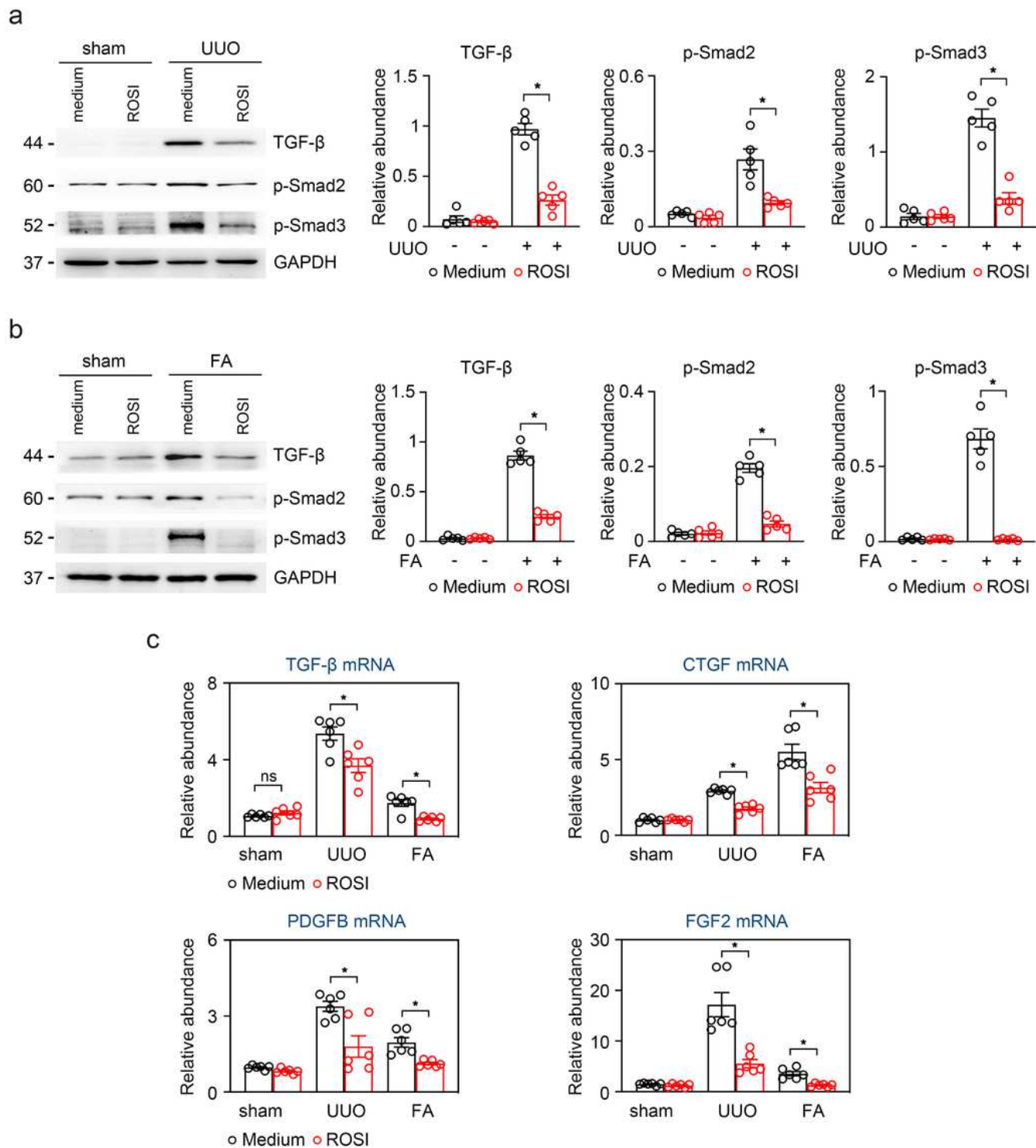
Figure 5

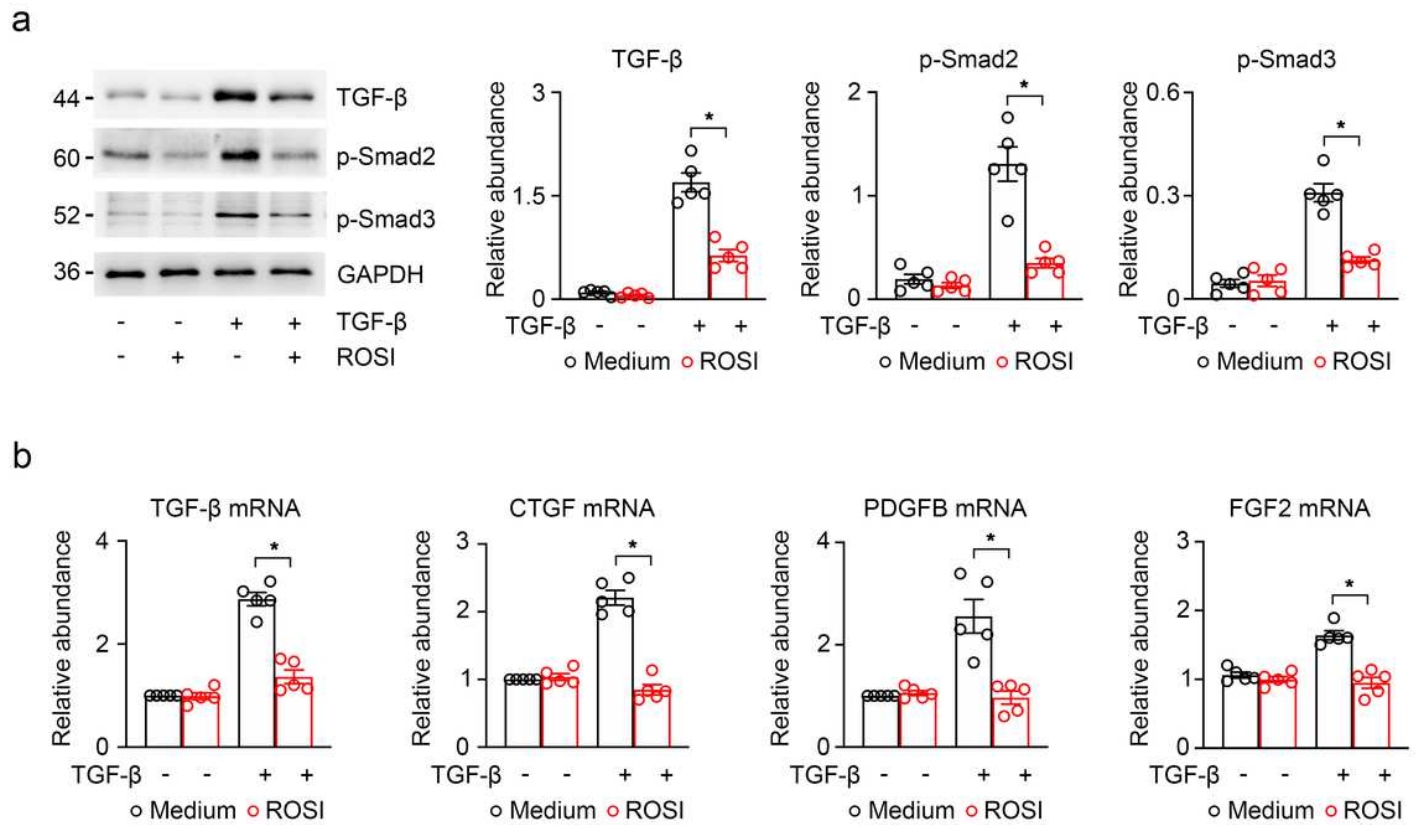ACSL4 inhibition improved the fibrosis reaction in TGF-β-induced HK-2 cells.(a) The representative images (six visual fields for each sample analyzed) of immunofluorescence staining for fibronectin and α-SMA (green) in the indicated group. The positive areas of indicated protein were further presented in quantification. Scale bars: 50 μm. (b) Western-blot analyzing the expression of fibronectin, collagen-I and α-SMA in the TGF-β- induced HK-2 cells treated with or without ROSI (left panel). GAPDH sets as a loading

control. Schematic representation of band intensity of indicated proteins (right panel). (c) RT- qPCR for fibronectin, collagen-I and α-SMA transcripts in total RNA extracts of HK-2 cells with DMSO- or ROSI- treated normal and TGF-β-treated cells. The data were calculated from three independent experiments and expressed as the mean ± SEM. Representative images from more than three independent experiments are shown above. Data are presented as mean ± SEM. *P 0.05, ns means no statistical significance.

Figure 6

The release of profibrotic cytokines was significantly reduced in UUO and FA kidneys after inhibiting ACSL4. (a, b) Western-blot analyzing the expression of profibrotic cytokines TGF-β, p-Smad2 and p-Smad3 in UUO-and FA-treated kidney samples. The relative abundance of the indicated protein expression was normalized by GAPDH (right panel). n=5 mice. (c) Profibrotic cytokines TGF-β, CTGF, FGF2 and PDGFB mRNA detected by RT-qPCR analysis in UUO and FA-treated mice. n=5 mice.

Representative images from more than three independent experiments are shown above. Data are presented as mean ± SEM. *P 0.05, ns means no statistical significance.
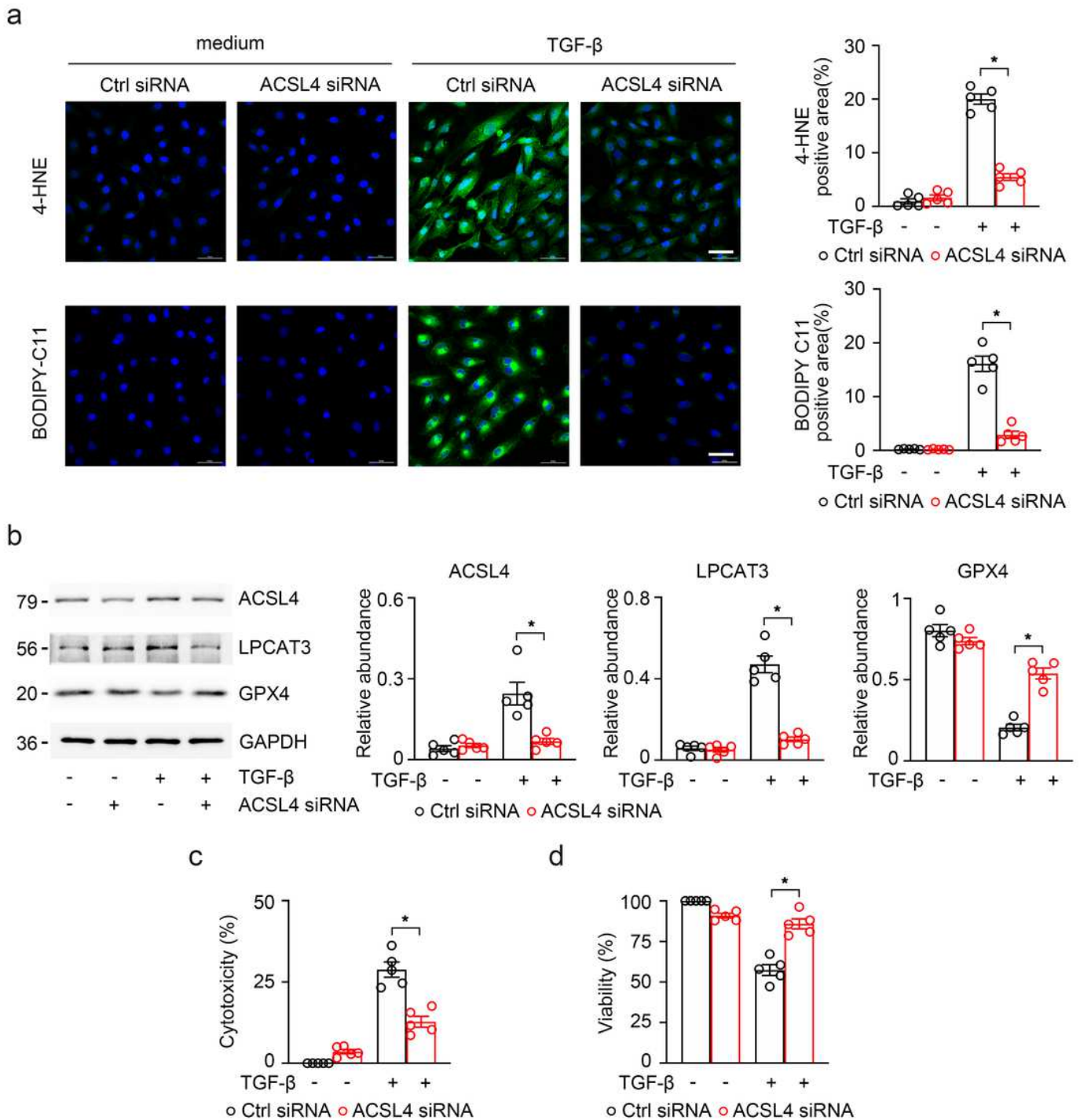

Figure 7

ACSL4 inhibition reduced profibrotic reaction in TGF-β-induced HK-2 cells. (a) Western-blot analyzing the expression of profibrotic cytokines TGF-β, p-Smad2 and p-Smad3 in TGF-β-induce HK-2 cells. The relative abundance of the indicated protein expression was normalized by GAPDH. Schematic representation of quantitative data of indicated proteins (right panel). (b) The expressions of profibrotic cytokines TGF-β, CTGF, FGF2 and PDGFB mRNA were analyzed by RT-qPCR in TGF-β-induced HK-2 cells. Representative images from more than three independent experiments are shown above. Data are presented as mean ± SEM. *P 0.05, ns means no statistical significance.
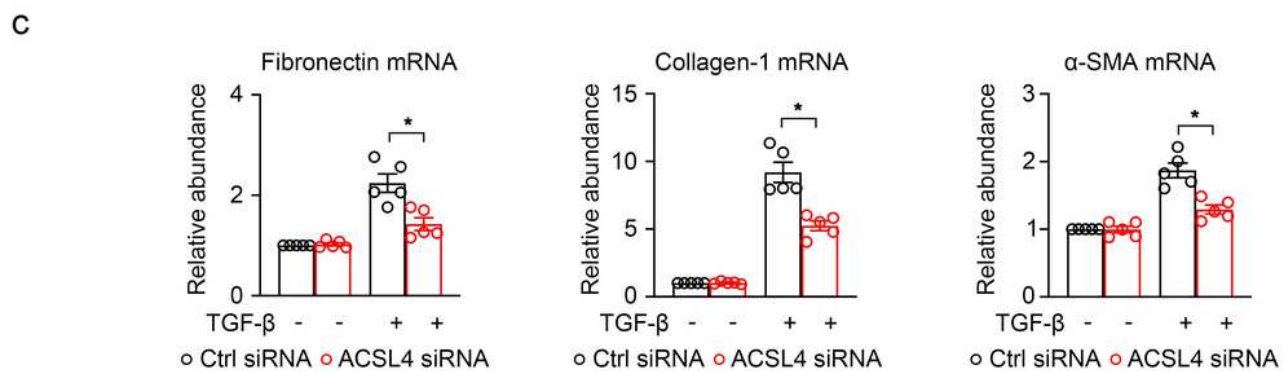
Figure 8

The knockdown of ACSL4 reduced TECs ferroptosis. (a)TGF-β-induced HK-2 cells treated with ROSI or DMSO were labeled with BODIPY 581/591 C11 and immunofluorescence stained with 4-HNE. Quantitative images to depict fluorescence intensity at the right panel. Scale bar = 50 μm. (b) Western-blot analysis of ACSL4, LPCAT3 and GPX4 in TGF-β-induced HK-2 cells. Schematic representation of quantitative data of indicated proteins (right panel). Representative images from three independent

experiments are shown above. n=5 mice. (c, d) Cell viability and cell cytotoxicity were assayed by MTT and LDH respectively. Both demonstrated a significant change in TGF-β-induced HK-2 cells with the knockdown of ACSL4. Representative images from more than three independent experiments are shown above. Data are presented as mean ± SEM. *P 0.05, ns means no statistical significance.
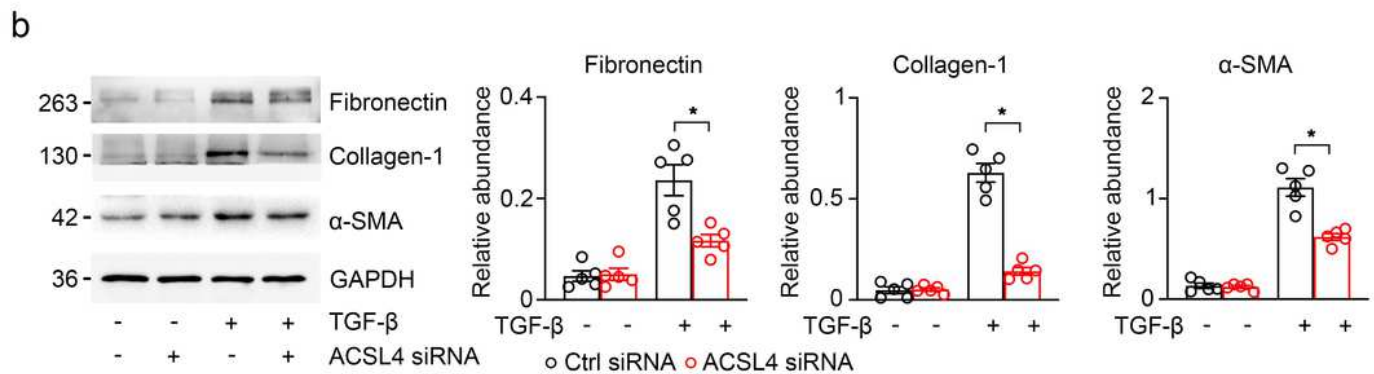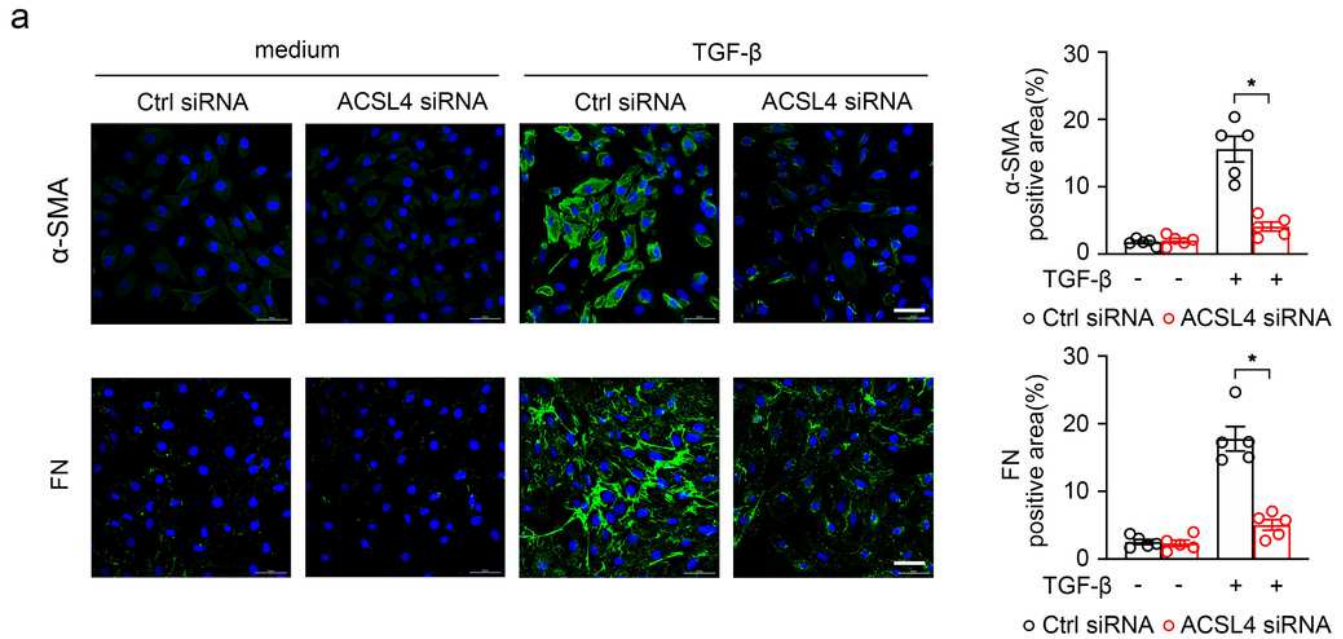
Figure 9

Knock ACSL4 down alleviated the progression of kidney fibrosis. (a)The representative image (six visual fields for each sample analyzed) of immunofluorescence staining for fibronectin and a-SMA (green) in the indicated group of HK-2 cells. The positive areas of indicated protein were further presented in quantification (right panel). (b)Western-blot analyzing the expression of fibronectin, collagen-I and α-SMA in the TGFβ-induced HK-2 cells with or without the knockdown of ACSL4 (right panel). GAPDH sets as the loading control. Schematic representation of band intensity of indicated proteins (left panel). (g) The expression of fibronectin, collagen-I and α-SMA detected by RT-qPCR in TGF-β-induced HK-2 cells with or without the knockdown of ACSL4. Representative images from more than three independent experiments are shown above. Data are presented as mean ± SEM. *P 0.05, ns means no statistical significance.
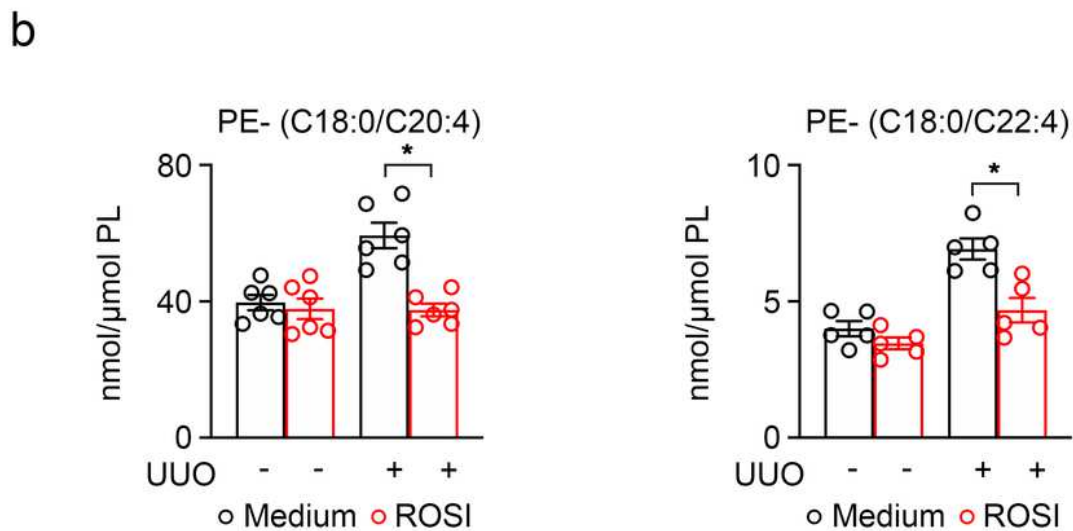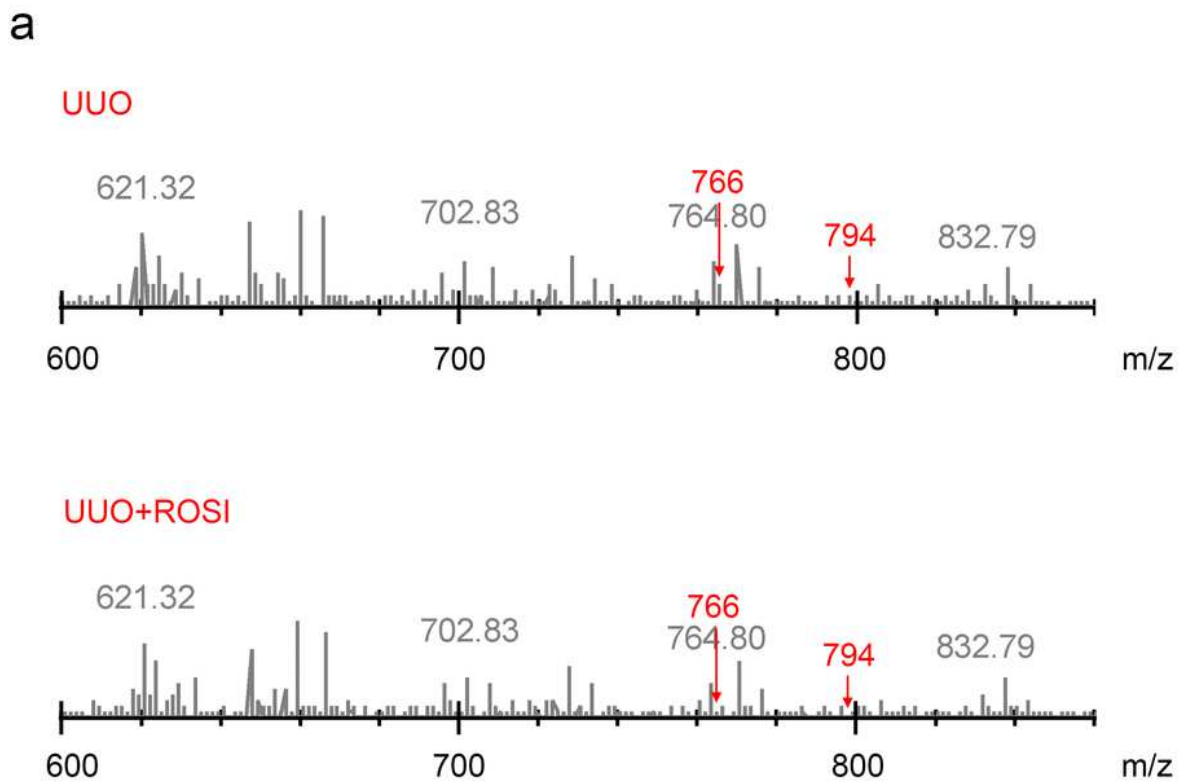
Figure 10

ACSL4 knockdown inhibited the PE ferroptotic precursors in kidney fibrosis response. (a) Quantitative assessment of PE molecular species (C18:0/C20:4 and C18:0/C22:4) in UUO kidney treated with ROSI. Data are presented as mean ± SEM. n = 6 mice. (b) Levels of AA-PE and AdA-PE in UUO kidney with or without ROSI. n = 6 mice. Data are presented as mean ± SEM. *P 0.05, ns means no statistical significance.

Supplementary Files

This is a list of supplementary files associated with this preprint. Click to download.

- SupplementaryFile.Originalwesternblots.pptx
- SupplementaryTable1.xlsx